IEEE Access
Multidisciplinary ⋮ Rapid Review ⋮ Open Access Journal

Received 24 July 2023, accepted 8 August 2023, date of publication 11 August 2023, date of current version 17 August 2023.

Digital Object Identifier 10.1109/ACCESS.2023.3304333

RESEARCH ARTICLE

Optimization of PI-Cascaded Controller's Parameters for Linear Servo Mechanism: A Comparative Study of Multiple Algorithms

M. ABDELBAR, HUDA RAMADAN, ABDELRAHMAN KHALIL, HAMAD FARAG, MAZEN BAHGAT, OMAR RABIE, AND YASSER EL-SHAER

Mechanical Engineering Department, Arab Academy for Science and Technology and Maritime Transport, Smart-Village Branch, Cairo 3650111, Egypt

Corresponding author: M. Abdelbar (mohamedhelmy1@aast.edu)

ABSTRACT In numerous industries, especially in automation and industrial processes, the linear servo mechanism is used. However, the parameters of the friction and backlash models are frequently unknown for servomechanism systems, resulting in system uncertainty. High steady-state inaccuracy is caused by friction, whereas undesired vibration is caused by blowback. In servomechanism systems, friction is an issue that is still not sufficiently addressed by a realistic model. To address these challenges, this research on the linear servo system is controlled by a proportional-integral (PI-Cascaded) controller, which enables systems to respond more rapidly, reduce or reject disturbance, and arrive at a steady state more quickly. Moreover, the controller's parameters are crucial to getting the best performance from a particular controller. As a result, the controller settings were adjusted using four different meta-heuristic optimization algorithms: Surrogate Based Optimization (SBO), Hybrid Genetic Pattern Search Algorithm (HGSPA), Particle Swarm Optimization (PSO), and Simulated Annealing (SA) with four objective functions: Integral Square Error (ISE), Integral Absolute Error (IAE), Integral Time Square Error (ITSE), and Integral Time Absolute Error (ITAE). Throughout the system's experimental testing, 50 cm was employed as the reference input. Negligible overshoot, quick rise and settling times, and excellent responsiveness are all characteristics of the PSO algorithm with ITSE objective function. Moreover, to assess the system's robustness. A 50 N force was applied to the system, and a sine wave signal is input into the system. The system shows remarkable stability and resilience throughout the 50 N load experimentation test.

INDEX TERMS Cascaded controller, genetic algorithm (GA), linear servo mechanism, optimization, particle swarm optimization (PSO), simulated annealing (SA), surrogate based optimization (SBO).

I. INTRODUCTION

The linear servo mechanism is widely utilized in industries, particularly in automation and manufacturing processes. Pick-and-place systems, tool-feeding systems used in the machining process, and indexing of operations like drilling, stamping, and embossing are a few examples of applications. It gained popularity as a linear-positioning tool due to the combination of its actuator's strengths and the simplicity of servo units' positioning control [1], [2], [3]. Moreover, the motion control system includes position servo control, which is significant. It requires accurate coordinate position control of moving parts, fast and precise motion, and a complete duplicate of the input position quantity and its changing trajectory in the output position quantity. In other words, primary control objectives are optimum position control precision, optimum position tracking accuracy, and sufficient tracking speed [4], [5].

However, for servomechanism systems, the parameters of the friction and backlash models are often not known, leading to system uncertainty [6]. Friction results in high steady-state inaccuracy, whereas blowback results in undesired

The associate editor coordinating the review of this manuscript and approving it for publication was Shih-Wei Lin.

vibration [7]. The friction problem in servomechanism systems has not yet been well explained by a realistic model [8].

As a result, several different types of controllers, including the popular Proportional-Integral-Derivative (PID) controller and its variations, have been proposed to enhance the positional and speed control of servo systems. PID controllers are frequently used in industrial process control to provide good results with a basic algorithm. It is simple for operators to understand and use in all industrial applications [9]. Conventional PID controllers are well-known for performing poorly when influenced by disturbances, despite being widely accepted in the industry [10]. Furthermore, servo control is the process of adjusting a motor's speed and position based on a feedback signal. The most fundamental kind of servo loop is the velocity loop. To reduce the error between the velocity command and velocity feedback, the velocity loop generates a torque command. Motor control is the process of delivering real torque in response to servo control loop torque orders. There has been a lot of work put into analyzing the servo systems since it takes time to adjust PID controllers for positional control systems. Servo systems often need a controller in addition to speed control, which is again usually done by cascading or connecting a position loop and a speed loop in sequence. In the lack of an explicit velocity loop, a single PID position loop is occasionally utilized to provide position and speed control [11], [12]. To improve performance, PID controllers are widely integrated into advanced control systems.

Cascade control is a type of advanced control system, which helps systems respond faster, decrease, or reject disturbance, provide robustness, and reach a steady state more quickly. In industrial operations, cascade control is usually applied. It resulted from its efficiency, robustness, and ease of use [13]. The primary loop (outer) and the secondary loop (inner) make up the cascade control system. It has two feedback loops, where the set point in the secondary loop will be represented by the output of the first loop controller. The secondary loop controller's signal output goes straight to the actuator, such as a control valve or electric motor.

In conventional cascade control, main and secondary loop controller parameters are tuned in sequence. The secondary controller's parameters are first tuned according to a set of guidelines, while the primary loop is in an open loop state. Moreover, the primary loop's controller parameters are adjusted by taking the controlled secondary loop's impact into account. There will be a recurrence if the outcomes are unsatisfactory. Moreover, the primary loop's controller parameters are adjusted by taking the controlled secondary loop's impact into account. There will be a recurrence if the outcomes are unsatisfactory. Therefore, PID-cascaded control tuning is more challenging and time-consuming [14]. Moreover, the fact that the controller gains vary based on the operational mode, the load applied to the system, and friction drifts or mechanical component loosening provide one of the obstacles in regulating and optimizing such systems. Frequently, the controller settings are set to conservative levels to prevent frequent re-tuning, which compromises the system's performance while preserving stability for a variety of loads [15].

Numerous techniques, including trial-and-error, D-partitioning, Ziegler-Nichols, and pole placement, have been developed since the development of PID controllers for the gain tuning of PID-controlled systems [16]. However, to be used effectively, most of these direct approaches need a thorough understanding of the system and its frequency response because they were created for linear, time-invariant systems.

The weighted tuning strategy was used by Meshram and Kanojiya [17] to fine-tune the PID controller for DC motor speed control. The Ziegler-Nichols tuning formula and modified Ziegler-Nichol PID tuning formula were used to adjust the PID parameters after creating the DC motor model in MATLAB. Based on output responsiveness, minimal settling time, and least overshoot, the two approaches were contrasted. Fajuke and Raji [18] offer a method for controlling the speed of a DC motor based on tweaking the PID parameter using conventional ZN. The DC shunt motor's speed control study was done to reduce the transient response parameters selected for the motor's improved speed response. The Simulink environment in MATLAB is used for the development of mathematical models of the motor. Additionally, Dursun and Durdu [19] investigated the sliding mode control (SMC) technique for controlling the speed of DC machines. The machine was put under different loading conditions, and the response is contrasted with a PID control method that is frequently employed. Reference [20] proposed a proportional-integral (PI) and Petri nets-based series multi-cell chopping controller for regulating a DC motor's speed. The multi-cell converter's capacitor voltage was kept constant while the armature current was controlled using the Petri Nets controller. To calculate the motor's switch reaction, binary control switches were also produced using the Petri Nets controller. MATLAB SimPower is used to model the system. However, the speed response of many of these standard ways hasn't been able to successfully regulate the motor. This is due to their inability to allow the diversity of restrictions to the fundamental design parameters, including overshoot and settling time [19]. The high computing time and high mathematical complexity of many standard approaches are another problem. Additionally, it should be highlighted that the design of any classical PID transforms into a challenging combinatorial issue that can only be resolved with the aid of optimization techniques [21].

These findings have led to the employment of a variety of meta-heuristic optimization techniques for PID controller gain tuning in nonlinear systems like robotic systems [22]. To further analyze the issue, it is imperative to submit any present solutions.

Many innovative approaches have been developed by researchers to adjust PID parameters, such as the Genetic Algorithm (GA) [23], Particle Swarm Optimization

(PSO) [24], Harris Hawk Optimization [25], Simulated Annealing [26], Surrogate Optimization [27], and Hybrid Genetic Pattern Search Algorithm (HGPSA) [28]. Köse et al. developed an optimal controller for the AVR system [29]. Moreover, Khosravi et al. developed a data-driven tunning approach for cascaded control [15]. Furthermore, Biyanto et al. introduced Simultaneous Optimization of tuning PID cascade control system [13]. To adjust the PID controller's parameters, Habib et al. [30] applied an improved whale optimization algorithm (IWOA). The suggested approach was used to select the proper controller parameter values to enhance the machine's transient responsiveness. To prove the viability of the suggested strategy, a comparison with different meta-heuristic methods was made. Suman and Giri [31] look at the speed control of a DC motor based on the application of soft computing techniques like fuzzy logic controller and PSO for PID controller parameter tuning. An ideal fuzzy PID controller architecture, based on traditional PID control and nonlinear variables employing the GA, was put out by Sultan and Jarjes [32]. Fuzzy logic controllers substantially increase the effectiveness of the algorithm by acting as one individual in the initial population of GA.

This paper provides a complete dynamic model for a linear servo system. A cascaded controller is furthermore implemented for the system. To assess the performance of the system, a thorough comparative analysis of several optimization approaches with various objective functions is also conducted for PI-Cascaded controller parameters tuning. These approaches have demonstrated exceptional results when used to solve various optimization problems. Additionally, the algorithm's key advantages are its simplicity and the harmony it creates between the exploitation and exploration stages. To determine the system's robustness, it was both simulated and experimentally tested using a range of loads and inputs.

This paper has the following structure. System Structure and Model which includes the mathematical modeling of the system, the control structure, and the dynamic model of the linear servo mechanism are detailed in Section II. Section III includes the optimal controller structure, and different objective functions used, and briefly describes the different optimization techniques. Section IV begins with the simulation results of an optimum controller that was used with various approaches and objective functions, is followed by experimental results, and is concluded with a comparative analysis of the outcomes of the experiments. The paper is concluded in Section V with a review of the result and possible future work.

II. SYSTEM STRUCTURE AND MODEL

Many industrial and scientific applications requiring precise control over the position and speed of a moving item employ linear servo mechanisms. Such systems frequently use linear actuators based on ball screws or lead screws. These actuators have certain drawbacks, including high cost, poor efficiency, and a limited stroke length [33]. Belt-driven V-Slot linear actuators have become an efficient means to get around these restrictions [34]. Compared to conventional linear actuators, V-Slot profiles provide several benefits, including cheap cost, high efficiency, and limitless stroke length. In this research, a control scheme is suggested for a belt-driven V-Slot 20 × 40 linear actuator that allows for accurate control of the carriage plate's position and speed.

An electric DC motor, a timing belt, a carriage plate, and a V-Slot 20 × 40 profile are the components of the proposed control system. The carriage plate is guided along the profile's guideways by the timing belt, which is driven by the DC motor. The carriage plate may move on it and convey loads and the profile is fixed to a supporting frame. A microcontroller manages the system to achieve the required behavior and accuracy by controlling the motor's set voltage. The system has an incremental encoder that measures the carriage and motor's position and speed. Additionally, as a safety measure, infrared (IR) sensors were utilized for the movement restrictions. Figure 1. illustrates the linear servo cart system in detail.

A. MATHEMATICAL MODEL OF THE LINEAR SERVO CART SYSTEM

Applying Newton's second law of motion and D'Alembert's principle to the system, the relationship between the force provided to the cart by the DC motor and the resulting motion of the cart can be established, as in (1) [1]:

$$M\dot{v}_c(t) + F_{aj}(t) = F_{cart}(t) - B_c v_c(t) \tag{1}$$

M is the cart mass, $\dot{v}_c$ is the cart's linear acceleration, F_{aj} is the inertial force on the motor, B_c is the cart damping coefficient, and v_c is the cart's linear speed.

$$F_{aj} = \frac{\eta_g k_g J_m \dot{\omega}_m}{r} \tag{2}$$

η_g is the gearbox efficiency, k_g is the gear ratio, J_m is the rotor inertia, $\dot{\omega}_m$ is the rotor's angular acceleration, and r is the pulley radius.

$$v_c = r k_g \omega_m \tag{3}$$

F_{cart} is the force on the cart due to the motor's armature current.

$$F_{cart} = \frac{I_a k_t}{r} \tag{4}$$

where I_a is the armature current, and k_t is the motor torque constant.

Substituting (2), (3), and (4) into (1) can be rewritten as:

$$r k_g \dot{\omega}_m + \frac{\eta_g k_g J_m \dot{\omega}_m}{r} = \frac{I_a k_t}{r} - r B_c k_g \omega_m \tag{5}$$

Rearranging (5):

$$\dot{\omega}_m \left(M r^2 k_g + \eta_g k_g J_m \right) + B_c r^2 k_g \omega_m - I_a k_t = 0 \tag{6}$$

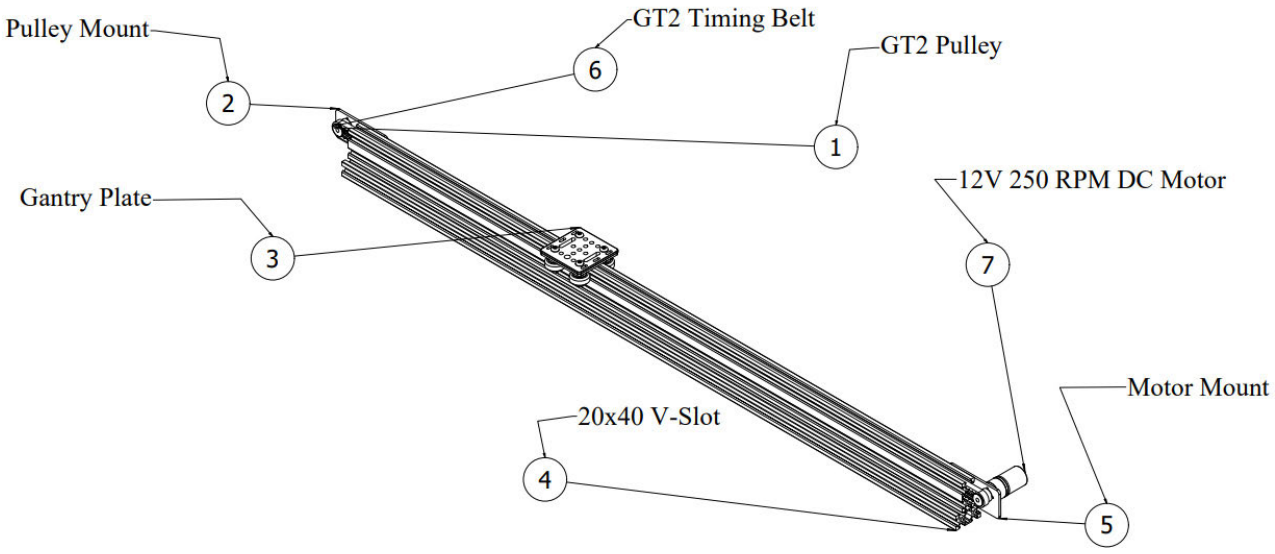

FIGURE 1. Linear servo mechanism CAD model.

Direct current motor circuit equation of motion derived using Kirchhoff's First Law:

$$L\dot{I}_a + RI_a - V_{in} + k_b\omega_m = 0 \tag{7}$$

The equivalent inertia term can be expressed as:

$$J_{eq} = \left(Mr^2k_g + \eta_g k_g J_m\right) \tag{8}$$

The equivalent damping term can be expressed as:

$$B_{eq} = B_c r^2 k_g \tag{9}$$

Finally, in a state space, the system can be described as:

$$\begin{bmatrix} \dot{I}_a \\ \omega_m \\ \theta_m \end{bmatrix} = \begin{bmatrix} \frac{-R}{L} & \frac{-k_b}{L} & 0 \\ \frac{k_t}{J_{eq}} & \frac{-B_{eq}}{J_{eq}} & 0 \\ 0 & 1 & 0 \end{bmatrix} \begin{bmatrix} I_a \\ \omega_m \\ \theta_m \end{bmatrix} + \begin{bmatrix} \frac{1}{L} \\ 0 \\ 0 \end{bmatrix} [V_{in}] \tag{10}$$

The state space equations, however, only describe the linear part of the system's behavior. The linear servomechanism provides considerable Coulomb friction to resist the motor's torque, measured to be up to half the operating range of the motor as an upper limit. This is represented by a dead zone block at the input to the state space equations, as the effective torque acting on the linear system is a result of the dead zone's output, which filters the PWM command below a certain threshold:

$$PWM_{effective} = \begin{cases} PWM_{command} - deadzone, \\ \qquad PWM_{commAnd} > deadzone \\ 0 \quad |PWM_{command}| \leq deadzone \\ deadzone - PWM_{command}, \\ \qquad PWM_{command} < -deadzone \end{cases} \tag{11}$$

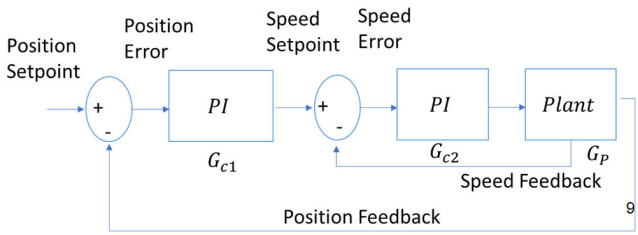

FIGURE 2. Configuration of cascade control [9].

This is then mapped appropriately to the corresponding motor voltage through the gain block between the dead zone block and the state space. Table 1 lists the parameters for the linear servo cart model.

TABLE 1. Parameters of the linear mechanism used.

Parameters	Values	Units
Motor armature resistance, R_a	4.204	Ω
Equivalent inertia, J_{eq}	0.0080606	kg. cm^2
Motor armature inductance, L_a	0.071478	H
Motor constant, K_t	0.031058	N. m/A
Equivalent viscous damping coefficient, B_{eq}	0.0020369	$N.s/rad$

B. THE CONTROL SCHEME

In the industry, the cascade control system is frequently used. Accelerating response times and enhancing dynamic performance are the two goals of cascade control systems [35]. The controller is made up of two cascaded loops, illustrated in Figure 2, each of which is in control of an individual component of the system. The system's linear position is controlled by the outer loop, while the speed of the system is controlled by the inner loop. The position controller is

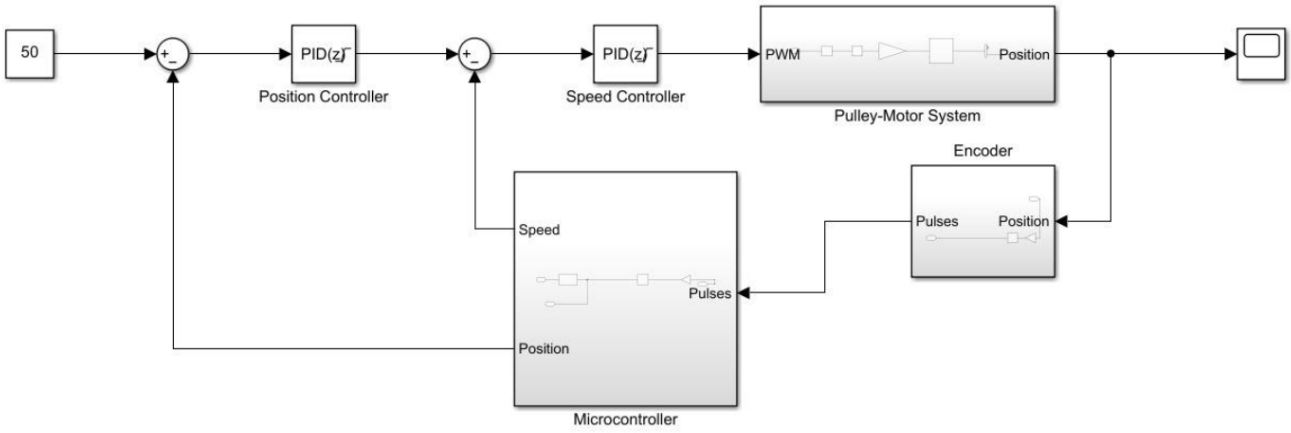

FIGURE 3. The entire dynamic model of the linear servo mechanism along with the cascaded controller.

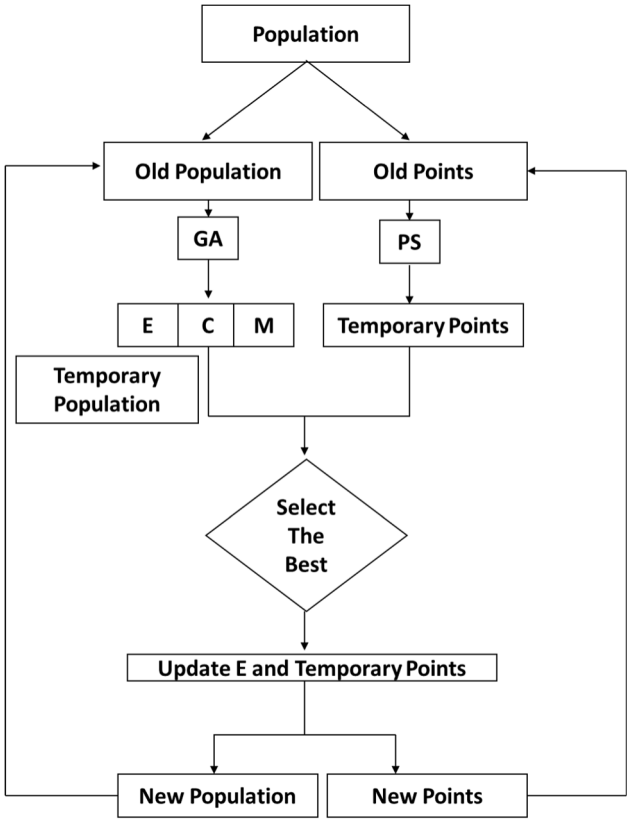

FIGURE 4. Flowchart of HGPSA [19].

designated by (12), while the speed controller is designated by (13) The controllers in both loops are PI controllers.

$$G_{C1}(s) = K_{p1} + \frac{K_{i1}}{s} \tag{12}$$

$$G_{C2}(s) = K_{p2} + \frac{K_{i2}}{s} \tag{13}$$

The motor-mounted encoder is used for feedback of both loops; feedback for the outer loop is obtained from the encoder's detected position, while feedback for the inner loop is differentiated in the meanwhile. The motor is controlled by a motor driver, which converts the speed controller's output, a voltage set point, to the motor's corresponding input voltage.

C. DYNAMIC MODELING OF THE LINEAR SERVO MECHANISM

Figure 3 illustrates the entire dynamic model of the linear servo cart system along with the cascaded controller. Moreover, to accurately represent the system as closely as possible and to ensure that any control approaches used in the model encounter the same challenges and conditions as the real model, the model's specific construction was done to reduce modeling errors [36]. The system's state space, which is explained in section II-A, is coupled with a dead zone block to approximate the dead zone, and this is known as the "Pulley-Motor System," which is the first component. To enhance the accuracy of this model, the second component, the encoder, models the encoder's resolution and quantization errors. Moreover, the encoder generates a square wave, the oscillations of which are counted by the microcontroller. Therefore, the pulse count must be an integer. The pulse count may then be calculated by multiplying the modeled position by the experimentally determined pulses per centimeter, which is 100.7, and then flooring the resultant value:

$$N_{pulses,i} = floor(100.7 \times X_{model,i}) \tag{14}$$

Microcontroller and control system: This simulates the signal processing portion of the dynamics of the system, introducing additional effects that may be present in real life that are introduced by differences as well as the computational time delay. The microcontroller can employ equation 13 to determine the speed as:

$$Pulse\ Rate = \frac{N_{pulses,i} - N_{pulses,i-1}}{T_{samp}} \tag{15}$$

Initialize population $\boldsymbol{Z} = \boldsymbol{Z_0} \in \mathbb{R}^{m \times n},\ \boldsymbol{z_i} \in \boldsymbol{Z},\ i \in \mathbb{N},\ 0 < i \leq n$

m *design variables, population size* n

for $t = 1$: *maximum generation*:

  population genetic algorithm (*chromosomes*):

    for $i = 1{:}\frac{n}{2}$:

      $\boldsymbol{x_i} = \boldsymbol{z_i}$

  population pattern search :

    for $i = \frac{n}{2} + 1{:}\, n$:

      $\boldsymbol{y_i} = \boldsymbol{z_i}$

  evaluate objective function $\boldsymbol{f(x_i)}$

  sort $\boldsymbol{x_i}$ *by* $\boldsymbol{f(x_i)}$ *then choose top k chromosomes*:

    $E = \{\boldsymbol{x_1}, \boldsymbol{x_2}, \boldsymbol{x_3}, \ldots \boldsymbol{x_k}\}$

  do crossover between chromosomes:

    for $i = 1{:}\frac{n}{2}$:

      choose random $j \in [1, n], j \neq i$

      $\boldsymbol{x_i} \leftarrow C(\boldsymbol{x_i}, \boldsymbol{x_j})$

  do mutations to chromosomes:

    for $i = 1{:}\frac{n}{2}$:

    $\boldsymbol{x_i} \leftarrow M(\boldsymbol{x_i})$

  $T_1 = \{\boldsymbol{x_1}, \boldsymbol{x_2}, \boldsymbol{x_3}, \ldots \boldsymbol{x_n}\}$

  for $i = \frac{n}{2} + 1{:}\, n$:

    pattern search on $\boldsymbol{y_i}$

  sort $\boldsymbol{y_i}$ *by* $\boldsymbol{f(y_i)}$ *then choose top k points*:

    $T_2 = \{\boldsymbol{y_1}, \boldsymbol{y_2}, \boldsymbol{y_3}, \ldots \boldsymbol{y_k}\}$

  Update new population:

  $\boldsymbol{Z} = T_1 \cup T_2$

FIGURE 5. Pseudo code of HGPSA.

The minimum measurable position would then be:

$$\delta x = \frac{1}{100.7} \approx 0.01cm \tag{16}$$

with the minimum measurable speed being:

$$\delta \dot{x} = \frac{200}{100.7} \approx 2\ cm/s. \tag{17}$$

This causes a quantization error that impacts the inner loop more than the outer loop since 2/16 $\sim$ 12.5% of the motor's operating range is subject to incorrect measurement. This can cause limit cycles in the system response, especially in regions where precise speed control is needed, such as during settling or an abrupt halt in the case of an aggressive controller.

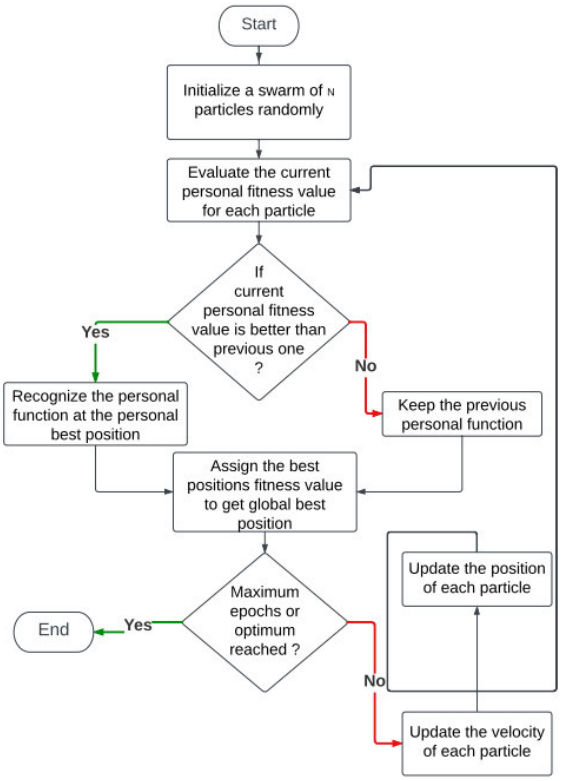

FIGURE 6. The flowchart of PSO [27].

Initialize population

for $t = 1$: *maximum generation*

  for i $= 1$: *population size*

    if $f(x_{i,d}(t) < f(p_i(t))$ ***then*** $p_i(t) = x_{i,d}(t)$

    $f\left(p_g(t)\right) = \min\left(f(p_i(t))\right)$

  end

  for d $= 1$: *dimension*

    $\boldsymbol{v_{i,d}(t+1)} = \boldsymbol{w v_{i,d}(t)} + \boldsymbol{c_1 r_1(p_i - x_{i,d}(t))} + \boldsymbol{c_2 r_2(p_g - x_{i,d}(t))}$

    $\boldsymbol{x_{i,d}(t+1)} = \boldsymbol{x_{i,d}(t)} + \boldsymbol{v_{i,d}(t+1)}$

    if $\boldsymbol{v_{i,d}(t+1) > v_{max}}$ ***then*** $\boldsymbol{v_{i,d}(t+1) = v_{max}}$

    elseif $\boldsymbol{v_{i,d}(t+1) < v_{min}}$ ***then*** $\boldsymbol{v_{i,d}(t+1) = v_{min}}$

    end

    if $\boldsymbol{x_{i,d}(t+1) > x_{max}}$ ***then*** $\boldsymbol{x_{i,d}(t+1) = x_{max}}$

    elseif $\boldsymbol{x_{i,d}(t+1) < x_{min}}$ ***then*** $\boldsymbol{x_{i,d}(t+1) = x_{min}}$

    end

  end

end

FIGURE 7. Pseudo code of PSO.

III. OPTIMAL PI-CASCADED CONTROL

To perform a comparative analysis of the optimum parameter tuning based on the linear servo mechanism PI-Cascaded controller, HGPSA, PSO, Simulated Annealing, and Surrogate Optimization techniques are applied with various objective functions.

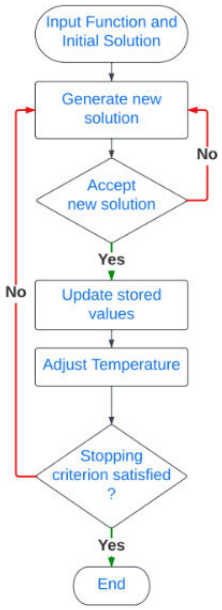

FIGURE 8. The flowchart of SA [28].

```
Initialize parameters
S = generate initial solution ();
T = T_0
while (T < T_final)
{
    Until (N ≤ 1 − Iter)
    {
        Generate solution S' in the neighborhood of S
            if f(S'') < f(S)
                S' to S
            else
                Δ = f(S') − f(S)
                r = random()
                if (r < exp(−Δ/k * T))
                S' to S
    }
    T = α × T
}
```

FIGURE 9. Pseudo code of SA.

A. HYBRID GENETIC PATTERN SEARCH ALGORITHM (HGPSA)

To present Pattern Search, Direct Search, a technique for addressing optimization issues without knowing the gradient of the objective function, needs first to be introduced [37]. GA is used for both global search and avoiding local minima. Because it converges too slowly, this is a drawback. PS, on the other hand, is a characteristic of local search but is sensitive to beginning values and is vulnerable to trap in local optima [38].

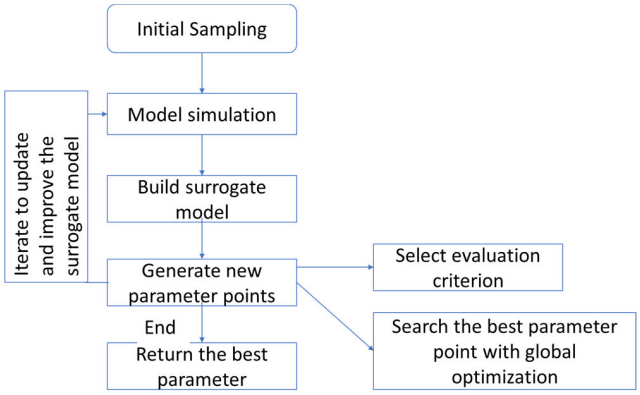

FIGURE 10. A flowchart of the surrogate-based optimization [30].

```
Initialization: Generate τ sample points
While the termination criterion is not met // The Surrogate-based local search part
Select τ best sample points x_1, x_2, ..... x_τ
Construct a local surrogate model f̂_i with τ selected sample points, locate the local range [lb_1, ub_1]
Generate x̂_best
Evaluate the exact function value of x̂_best
Best solution currently found x̂_best: FEs = FEs + 1 // The surrogate-guided prescreening part
Construct a global surrogate model f̂_g
Generate u_best
Evaluate the exact function value of u_best
Update database and the best solution found x̂_best: FEs = FEs + 1
End While
Output
```

FIGURE 11. Pseudo code of SBO.

The strong global search ability of GA and the excellent local search ability of PS must be combined to develop the hybrid genetic pattern search algorithm (HGPSA), which divides the population into two sub-populations, one of which executes the genetic algorithm and the other of which executes the pattern search [39]. Top results from each stage from the two subpopulations are gathered to update elite individuals. The schematic diagram of the method is shown in Figure 4.

Elite rate, crossover rate, and mutation rate are indicated in Figure 4 by the letters E, C, and M, respectively. The term "Elite" refers to the population's top performers, who are typically passed on directly to the following generation to ensure that the GA converges to the global optima. The HGPSA chooses the most competent individual to update the elite subpopulation and the temporary point after comparing the elite subpopulation by GA and the temporary point of PS.

The pseudocode of the HGPSA is shown in Figure 5.

Table 2 contains a list of the chosen parameters of the HGPSA.

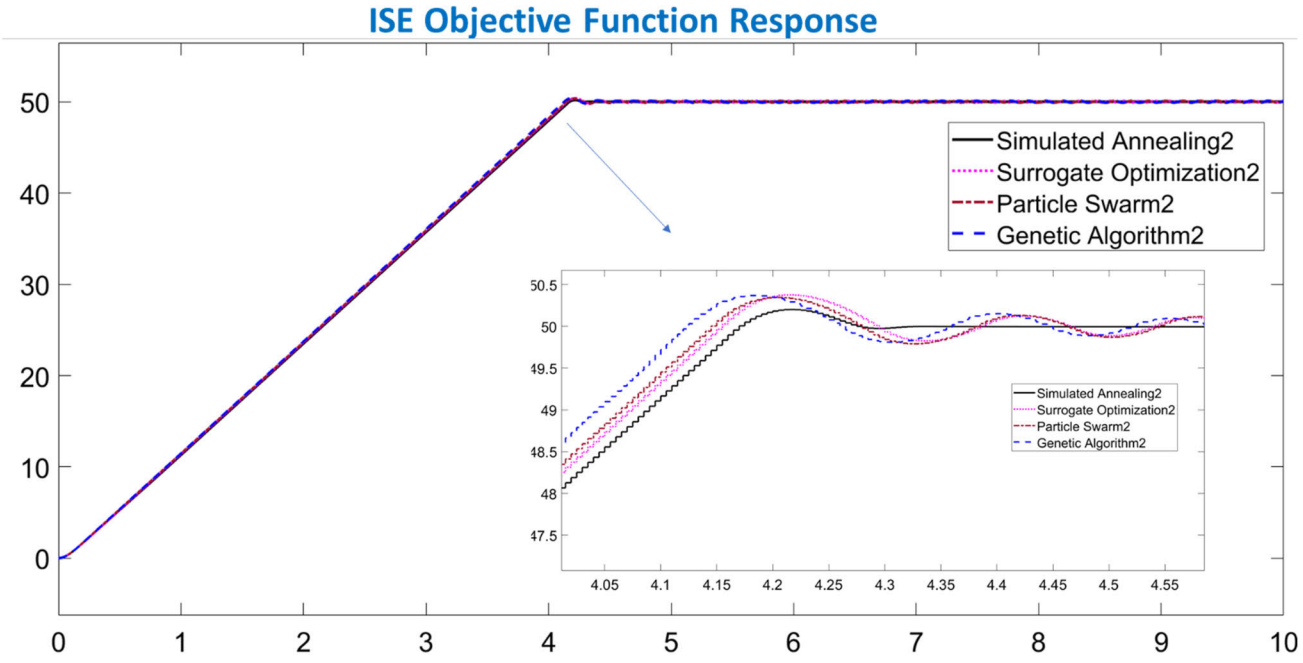

FIGURE 12. The simulation transient responses of different algorithms with the ISE objective function.

TABLE 2. Parameters of the HGPSA.

Parameters	Type/Value
Population Type	Double Vector
Population Size	50
Creation function	uniform
Scaling Function	Rank
Selection Function	Tournament
Mutation Function	Adaptive feasible
Crossover function	Constraint dependent
Migration direction	Forward

B. PARTICLE SWARM OPTIMIZATION (PSO)

The PSO [40] algorithm is based on how birds interact with one another. In this approach, a random population is first generated. Everybody is given a velocity and a tiny social network and is referred to as a particle. Fitness or objective function values are assessed for each particle. The personal ideal for each person, the global optimum for the whole population, and the neighborhood optimal discovered by each person's neighbors are all kept updating velocity and position for each person in PSO, which is based on fitness as opposed to GA. Until maximum generations or convergence are attained, this procedure is repeated. A flowchart illustrating the flux of PSO is shown in Figure 6.

The pseudocode of standard PSO is shown in Figure 7.

Table 3 contains a list of the chosen parameters of the PSO.

C. SIMULATED ANNEALING (SA)

The basis of SA [41] is the thermodynamics theory of liquids that crystallize when cooled. Populations are initialized, much like in other heuristic approaches, and a starting

TABLE 3. Parameters of the PSO.

Parameters	Type/Value
Inertia Range	[0.1, 1.1]
Neighborhood Size	0.25
Self-Adjustment Weight	1.49
Swarm Size	100

temperature is assigned to them. The population's whole population is examined for fitness. Now, using the temperature and a random number, a new population is created that is comparable to the older one, and their fitness is assessed. The best person is added to the existing population based on a comparison of the fitness differences between the old and new populations and the current temperature. Then the temperature is updated using a cooling plan. Up until the maximum number of generations or convergence is attained, this procedure is repeated. A flowchart illustrating the SA algorithm is shown in Figure 8, and the pseudocode of standard SA is shown in Figure 9.

TABLE 4. Parameters of the SA.

Parameters	Type/Value
Initial temperature	100
Re-anneal Interval	100
Function Tolerance	$1e^{-6}$

Table 4 contains a list of the chosen parameters of the SA.

D. SURROGATE BASED OPTIMIZATION

The aim of surrogate-based optimization (SBO), a class of optimization procedures that makes use of surrogate

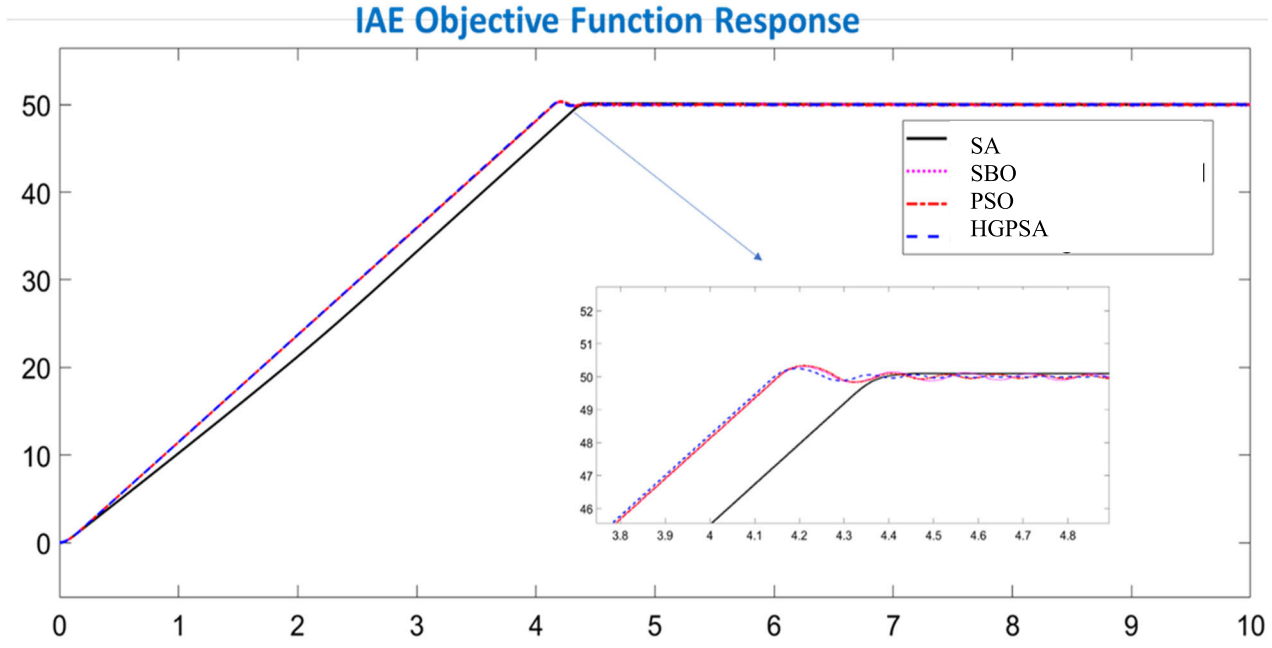

FIGURE 13. The simulation transient responses of different algorithms with the IAE objective function.

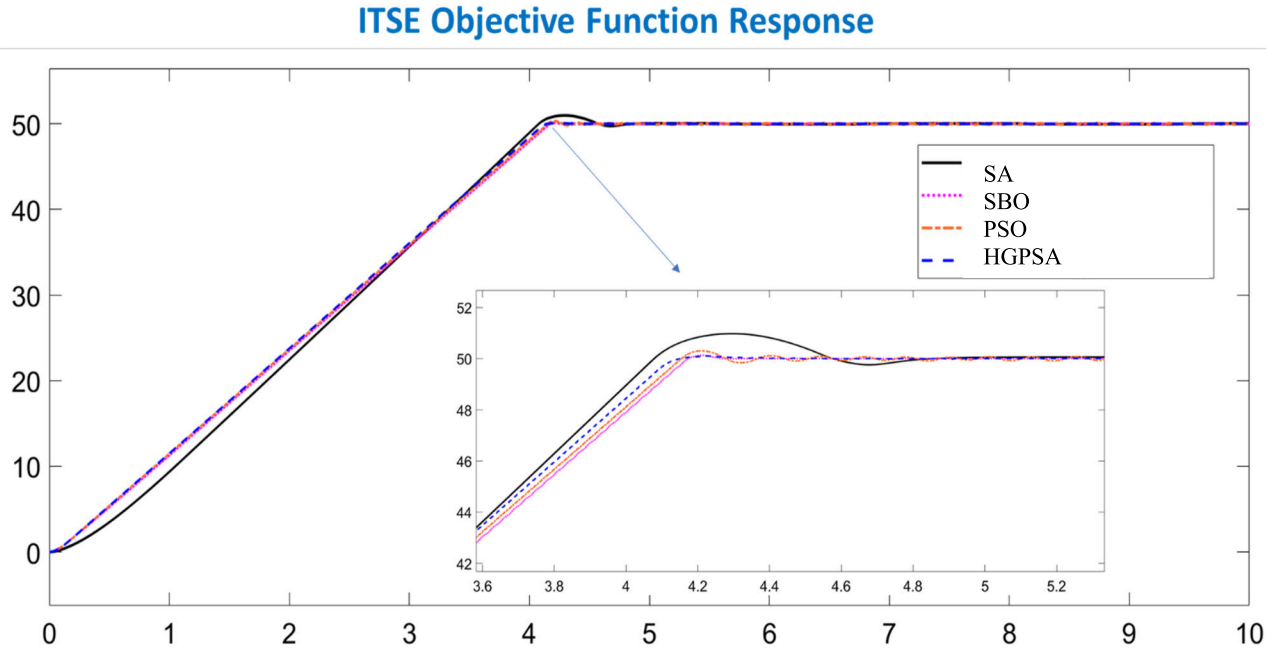

FIGURE 14. The simulation transient responses of different algorithms with the ITSE objective function.

modeling techniques, is to find the global minimum of an objective function while requiring a minimum number of possible evaluations of the objective function. The basic idea is to use a surrogate model that is easier to assess in place of the objective function to lower the computing cost of evaluating it. To do this, the algorithm attempts to find an appropriate equilibrium between two essential goals: exploration and speed [42]. It has been demonstrated that the technique, when applied to continuous objective functions on limited domains, converges to a global solution [43], [44]. A flowchart illustrating the SBO algorithm is illustrated in Figure 10, and the pseudocode of standard SBO is shown in Figure 11.

Table 5 contains a list of the chosen parameters of the SBO.

E. OBJECTIVE FUNCTIONS

For the evaluation of the controller's performance, choosing a suitable objective function (OF) for the optimization

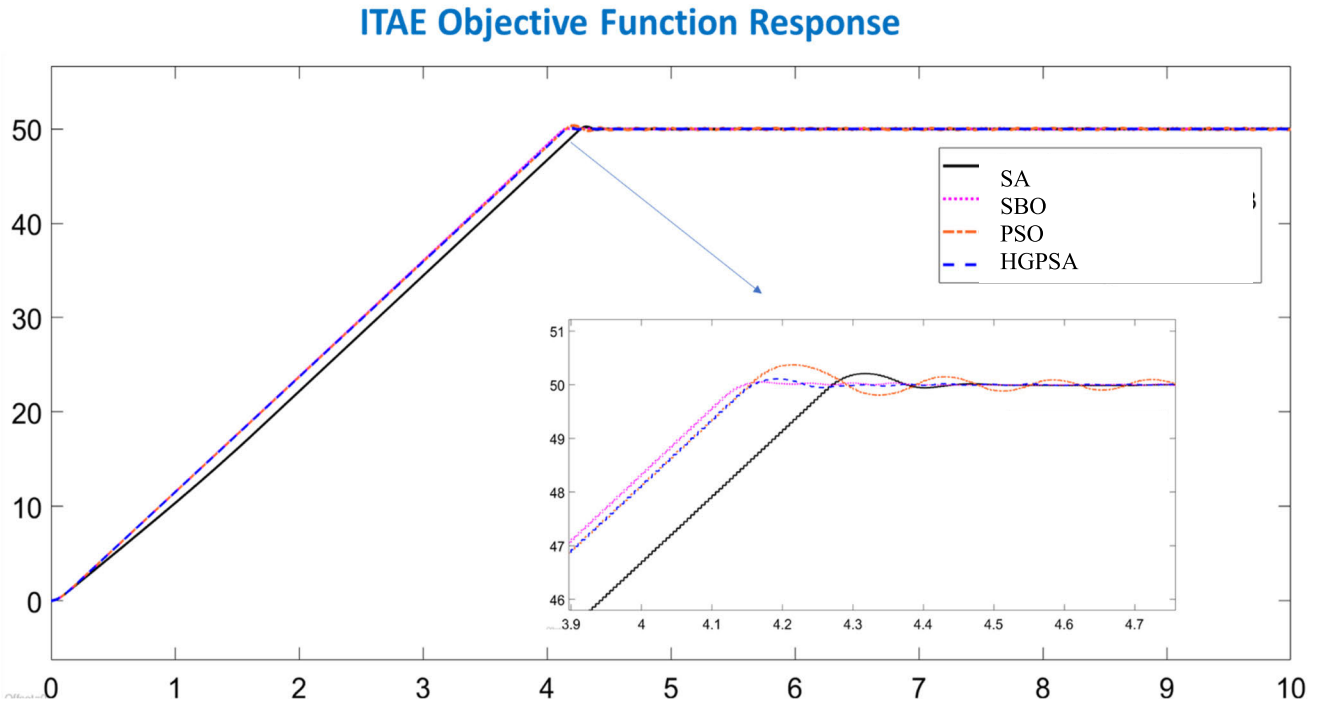

FIGURE 15. The simulation transient responses of different algorithms with the ITAE objective function.

TABLE 5. Parameters of the SBO.

Parameters	Type/Value
Min Sample Distance	$1e^{-6}$
Min Surrogate Points	20
Max Function Evaluations	200
Constraint Tolerance	$1e^{-3}$

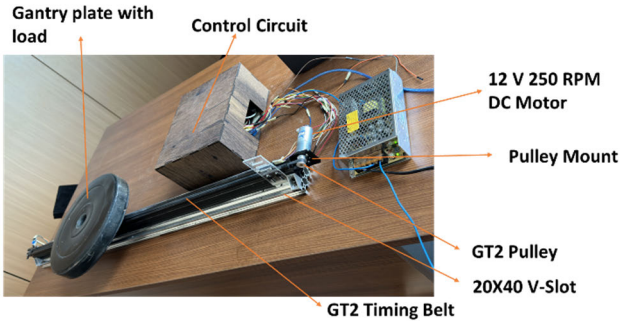

FIGURE 16. Block diagram of the experiment platform.

TABLE 6. PID parameters for different algorithms and different objective functions.

		Primary Loop		Secondary Loop	
Algorithm	Objective function	K_p	K_i	K_p	K_i
SBO	ISE	586	258	86	523
HGPSA	ISE	1000	725	1000	1000
PSO	ISE	446	333	829	694
SA	ISE	61	33	109	16
SBO	IAE	672	984	672	578
HGPSA	IAE	123	614	944	513
PSO	IAE	240	283	583	839
SA	IAE	21	0	67	37
SBO	ITSE	47	29	106	21
HGPSA	ITSE	25	197	1000	1000
PSO	ITSE	432	824	190	474
SA	ITSE	57	100	12	48
SBO	ITAE	40	194	1000	668
HGPSA	ITAE	55	957	611	123
PSO	ITAE	814	162	644	60
SA	ITAE	66	251	70	56

of the linear servo mechanism is essential. Where the goal is to identify the parameters that will minimize the chosen objective function. The many objective functions that have been chosen and applied to assess the design requirements and get the best possible control parameters for the mechanism are thoroughly discussed in this section. Integral square error (ISE) (18), integral absolute error (IAE) (19), integrated time absolute error (ITAE) (20), and integral time square error (ITSE) (21) are the four objective functions. The objective functions in this research were selected based on their relevance to the study's goals and are often used to assess the effectiveness of PID controller designs in the literature [29], [45], [46], [47].

A robust comparison and evaluation of the optimization approaches and algorithms used during this research are made possible using numerous objective functions, and this analysis will provide insight into the effectiveness of the

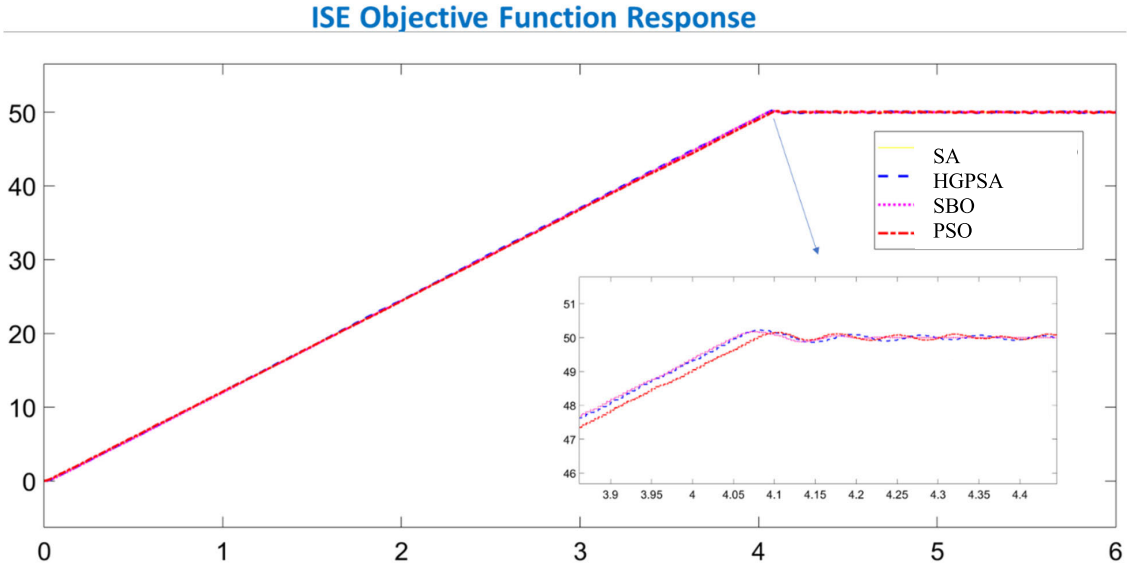

FIGURE 17. The experimental transient responses of different algorithms with the ISE objective function without load.

tuning methods and their effects on system performance.

$$ISE = \int_0^t [e(t)]^2 dt \tag{18}$$

$$IAE = \int_0^t |e(t)|\, dt \tag{19}$$

$$ITAE = \int_0^t t\,|e(t)|\, dt \tag{20}$$

$$ITSE = \int_0^t t[e(t)]^2 dt \tag{21}$$

TABLE 7. Simulation transient response for different algorithms and different objective functions.

Algorithm	Objective function	Overshoot (cm)	Peak Time (s)	Rise Time (s)	Settling Time (s)
SBO	ISE	0.31240	4.215	3.2800	4.325
HGPSA	ISE	0.27455	4.185	3.2597	4.310
PSO	ISE	0.26795	4.205	3.2757	4.340
SA	ISE	0.20265	4.215	3.2836	4.257
SBO	IAE	0.22565	4.205	3.2807	4.320
HGPSA	IAE	0.24850	4.190	3.2679	4.270
PSO	IAE	0.39110	4.210	3.2720	4.320
SA	IAE	0.08555	4.460	3.4440	4.470
SBO	ITSE	0.12885	4.210	3.2800	4.215
HGPSA	ITSE	0.10690	4.230	3.2533	4.250
PSO	ITSE	0.37395	4.205	3.2712	4.300
SA	ITSE	0.94005	4.295	3.0647	4.795
SBO	ITAE	0.07170	4.170	3.2606	4.215
HGPSA	ITAE	0.11545	4.190	3.2753	4.250
PSO	ITAE	0.40360	4.210	3.2735	4.350
SA	ITAE	0.20265	4.215	3.2836	4.405

IV. SIMULATION AND EXPERIMENTAL RESULTS

Table 6 lists the K_p and K_i parameters for the primary and secondary loops of the PID controller that are optimized using the HGPSA, PSO, SA, and SBO optimization algorithms with the ISE, IAE, ITSE, and ITAE objective functions.

TABLE 8. Experimental transient response for different algorithms and different objective functions without load.

Algorithm	Objective function	Overshoot (cm)	Peak Time (s)	Rise Time (s)	Settling Time (s)
SBO	ISE	0.26010	4.045	3.1803	4.114
HGPSA	ISE	0.15980	4.075	3.2145	4.150
PSO	ISE	0.04990	4.100	3.2600	4.113
SA	ISE	0.17000	4.065	3.2092	4.114
SBO	IAE	0.18005	4.040	3.1903	4.085
HGPSA	IAE	0.14995	4.070	3.2150	4.120
PSO	IAE	0.18990	4.050	3.1993	4.130
SA	IAE	0.14000	4.095	3.2225	4.150
SBO	ITSE	0.30050	5.030	3.8979	5.120
HGPSA	ITSE	0.14010	4.070	3.1948	4.102
PSO	ITSE	0.00000	4.250	3.2231	4.280
SA	ITSE	0.34055	4.785	3.7824	4.810
SBO	ITAE	0.24010	3.995	3.1572	4.061
HGPSA	ITAE	0.12005	4.075	3.2166	4.077
PSO	ITAE	0.09995	4.120	3.2856	4.157
SA	ITAE	0.14985	4.085	3.2158	4.148

TABLE 9. Experimental transient response for different algorithms and different objective functions with 50 N force.

Algorithm	Objective function	Overshoot (cm)	Peak Time (s)	Rise Time (s)	Settling Time (s)
SBO	ISE	0.10980	4.620	4.5082	4.689
HGPSA	ISE	0.11975	4.585	3.6463	4.657
PSO	ISE	0.24045	4.557	3.6037	4.623
SA	ISE	0.11010	4.625	3.6768	4.790
SBO	IAE	0.25035	4.595	3.6276	4.630
HGPSA	IAE	0.26030	4.600	3.6319	4.670
PSO	IAE	0.27065	4.740	4.2488	4.640
SA	IAE	0.10005	4.845	3.8250	4.847
SBO	ITSE	0.06995	4.610	4.5266	4.612
HGPSA	ITSE	0.07980	4.605	3.6506	4.610
PSO	ITSE	0.04990	4.620	3.6760	4.650
SA	ITSE	0.19010	6.125	4.8582	6.121
SBO	ITAE	0.35085	4.640	4.5066	4.720
HGPSA	ITAE	0.10990	5.591	4.2835	4.670
PSO	ITAE	0.01995	4.590	3.6566	4.680
SA	ITAE	0.21025	4.850	3.8519	4.912

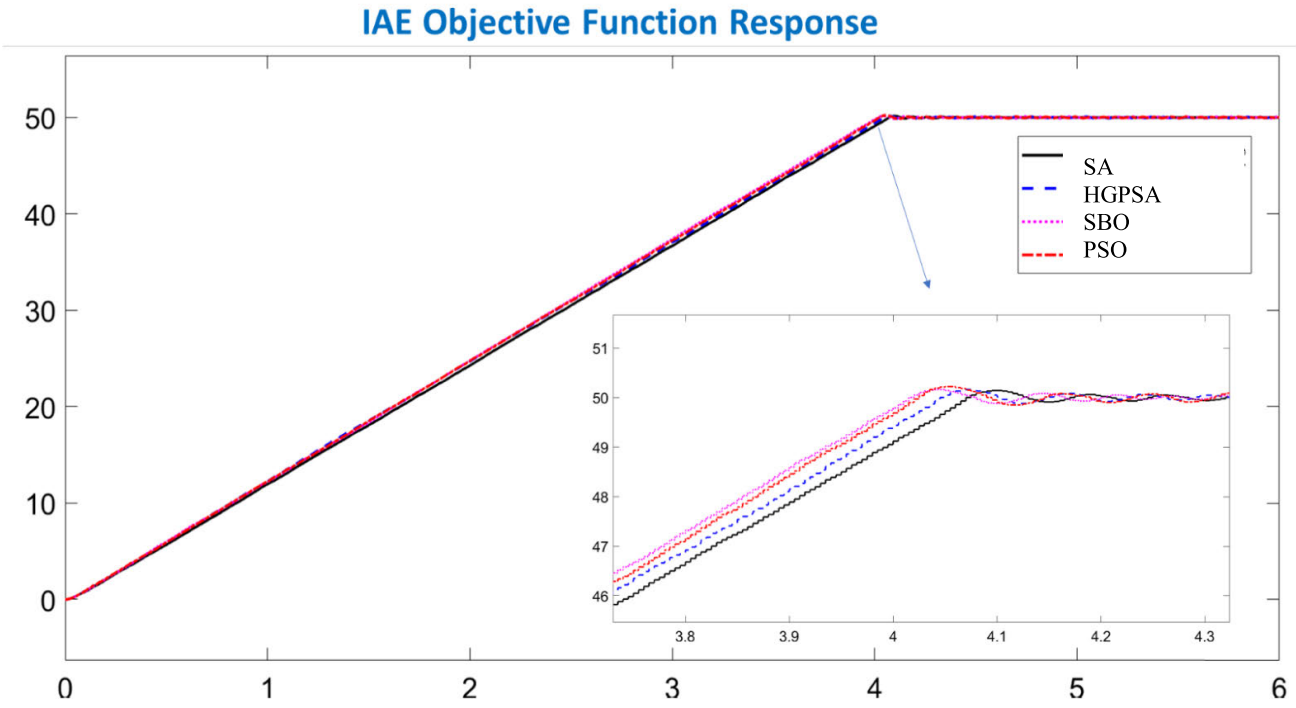

FIGURE 18. The experimental transient responses of different algorithms with the IAE objective function without load.

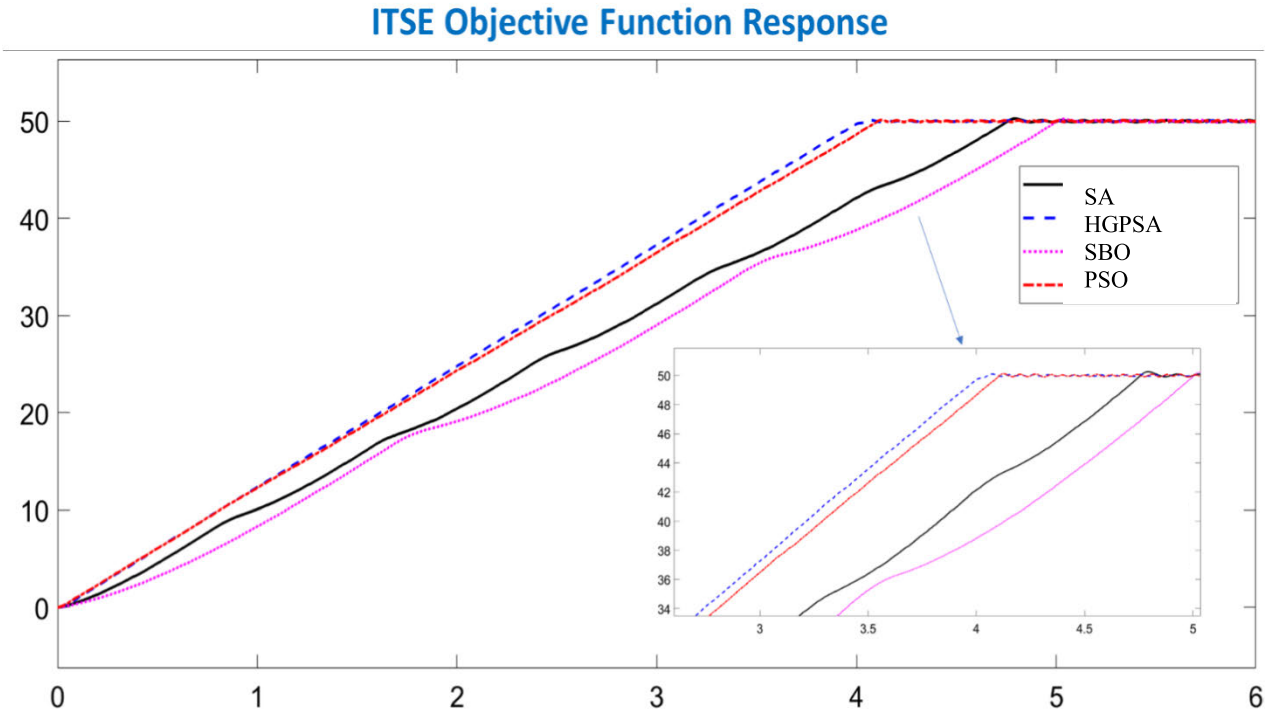

FIGURE 19. The experimental transient responses of different algorithms with the ITSE objective function without load.

A. SIMULATION RESULTS

The ISE, IAE, ITSE, and ITAE objective functions were used to obtain the HGPSA, PSO, SA, and SBO transient responses in Table 7 with 50 *cm* as a reference input to the system. In addition, Figure 12 shows the transient responses of different algorithms with the ISE objective function, Figure 13 shows the transient responses of different algorithms with the IAE objective function, Figure 14 illustrates the transient responses of different algorithms with the ITSE objective function, and Figure 15

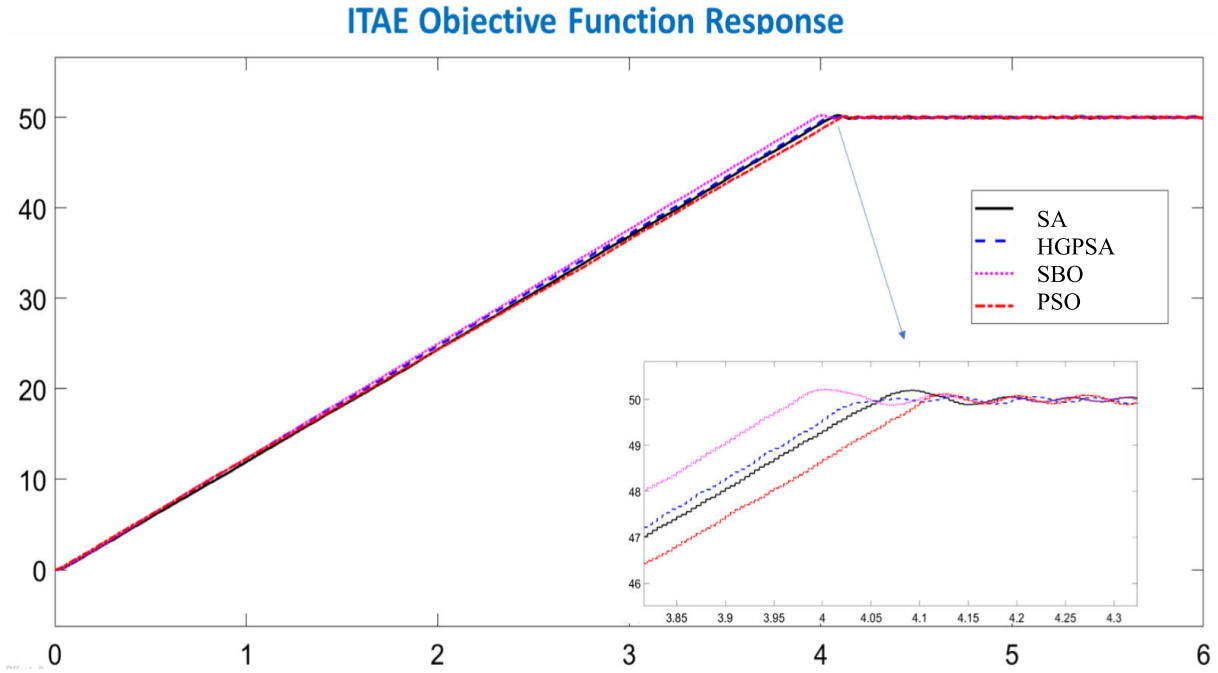

FIGURE 20. The experimental transient responses of different algorithms with the ITAE objective function without load.

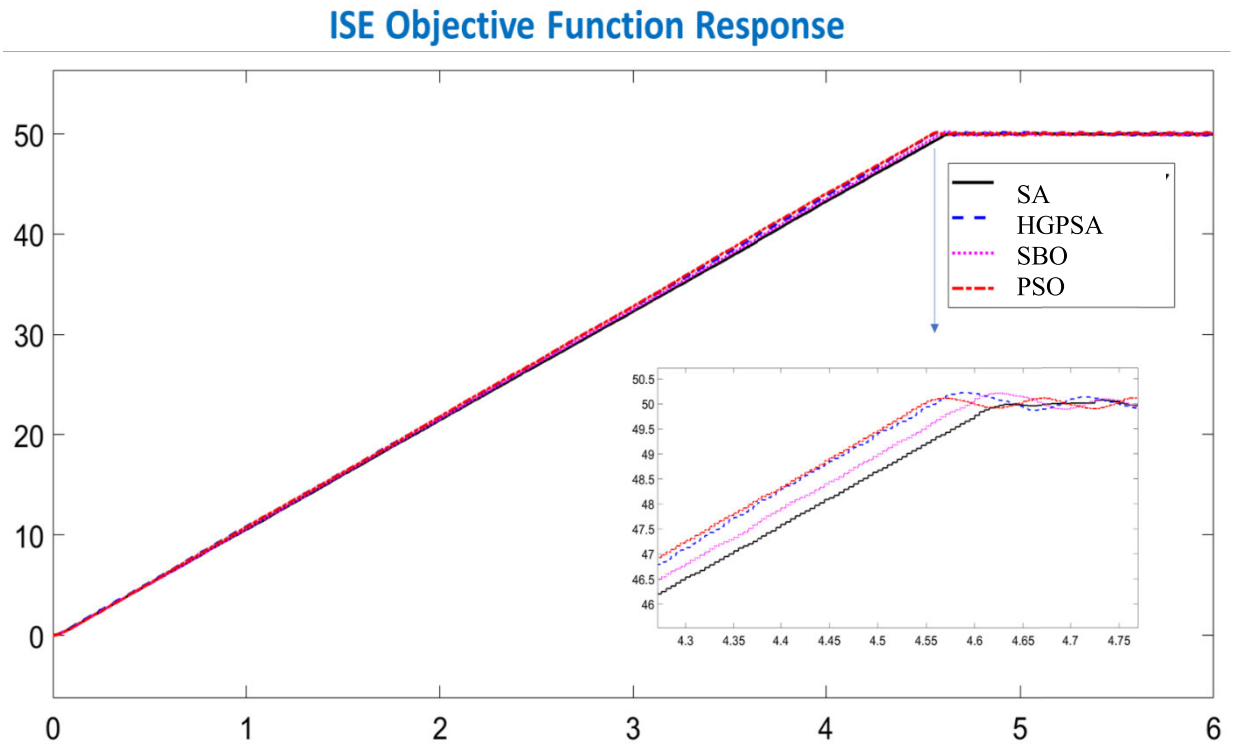

FIGURE 21. The experimental transient responses of different algorithms with the ISE objective function with 50 N load.

represents the transient responses of different algorithms with the ITAE.

The SA algorithm with IAE objective function generates an excellent response with 0.08555 *cm* overshoot, as shown by the system's transient responses, but the rise time and settling time are relatively long. This is primarily due to low proportional gain values in the inner and outer loops. The SBO with ITAE objective function, on the other

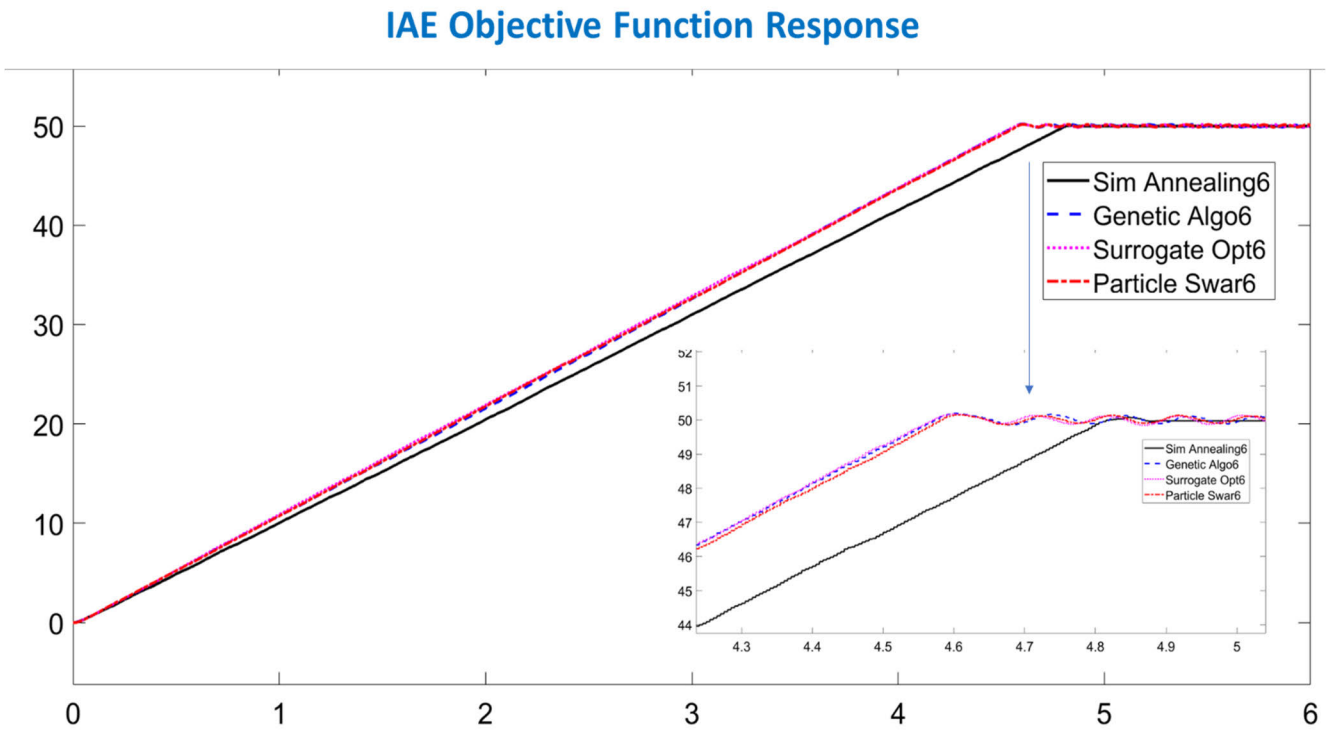

FIGURE 22. The experimental transient responses of different algorithms with the IAE objective function with 50 N load.

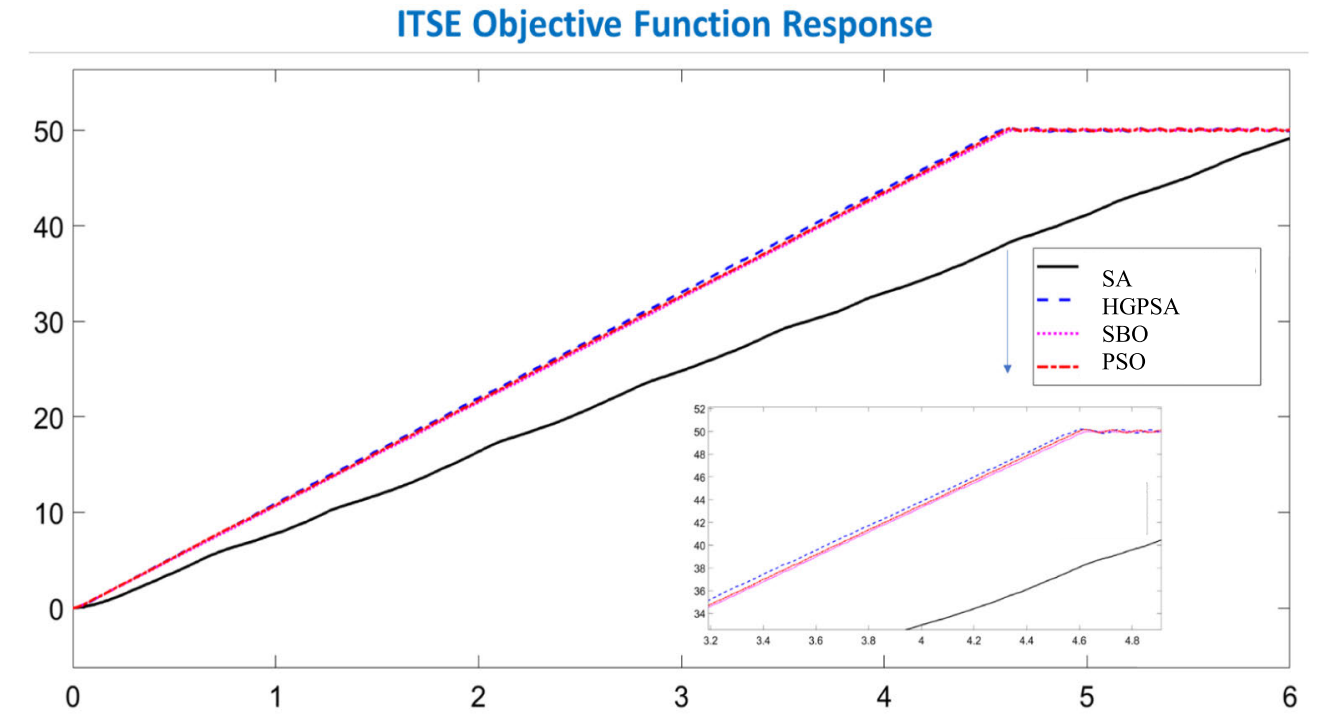

FIGURE 23. The experimental transient responses of different algorithms with the ITSE objective function with 50 N load.

hand, produces an excellent response with 0.07170 *cm* overshoot, 3.2606 *s* rise time, and 4.215 *s* settling time. The improvements in rise time and settling time are due to the high proportional gain value in the position controller loop.

B. EXPERIMENTAL RESULTS

The linear servo system proposed in this paper is verified by experiments, the hardware structure diagram of the system is shown in Figure 16.

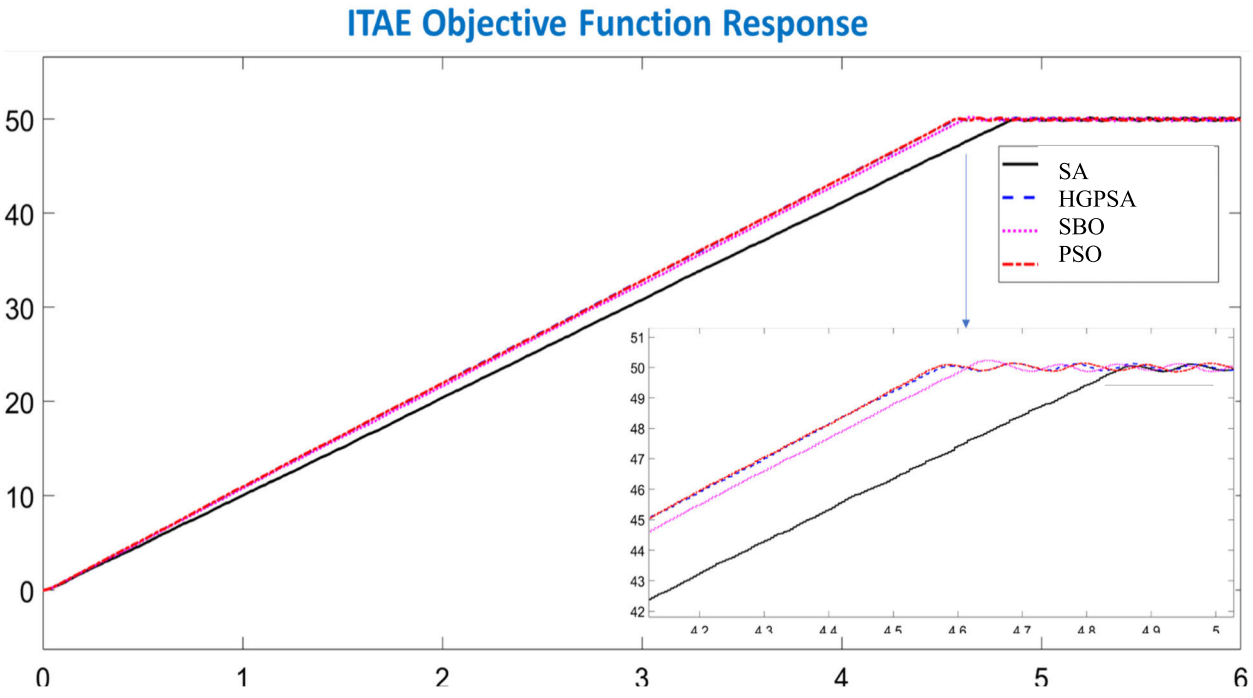

FIGURE 24. The experimental transient responses of different algorithms with the ITAE objective function with 50 N load.

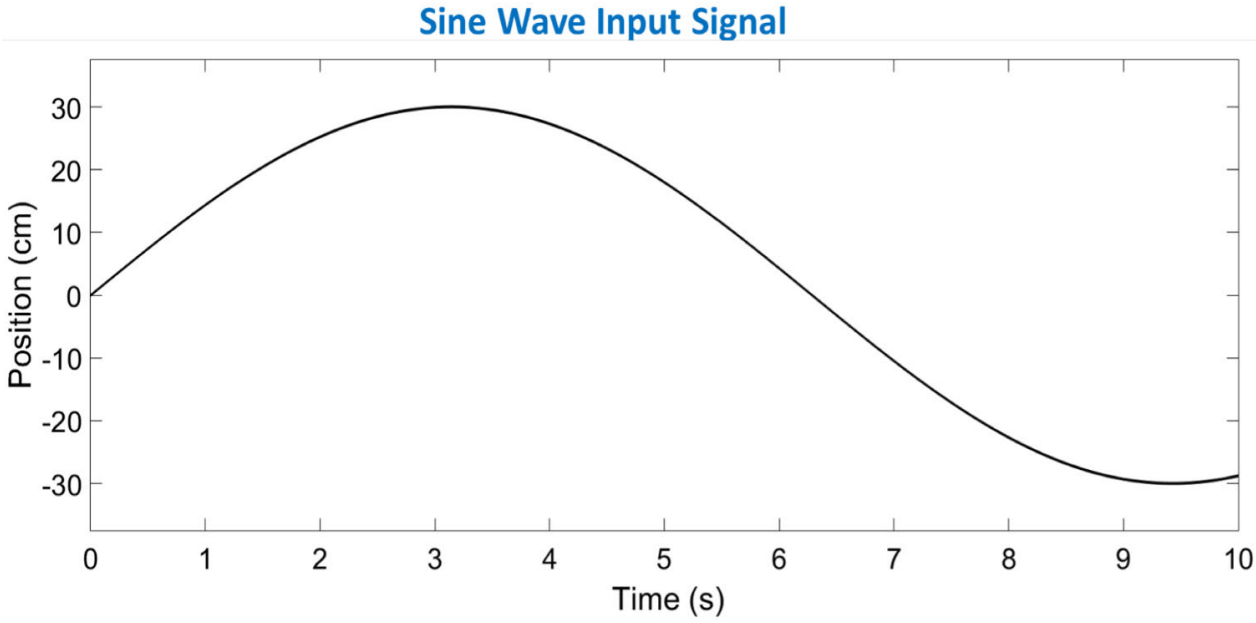

FIGURE 25. Sine wave input signal.

The system was subjected to experimental testing using the same simulation-based parameters. The HGPSA, PSO, SA, and SBO transient responses without load were obtained in Table 8 using the ISE, IAE, ITSE, and ITAE objective functions, with 50 cm provided as the system's reference input. Figure 17 shows the transient responses of different algorithms with the ISE objective function, Figure 18 shows the transient responses of different algorithms with the IAE objective function, Figure 19 illustrates the transient responses of different algorithms with the ITSE objective function, and Figure 20 represents the transient responses of different algorithms with the ITAE.

The system's simulation and experimental responses are quite similar. There are certain variations nevertheless because to signal noise, encoder resolution limitations, microcontroller specification, disturbances, and PID sat-

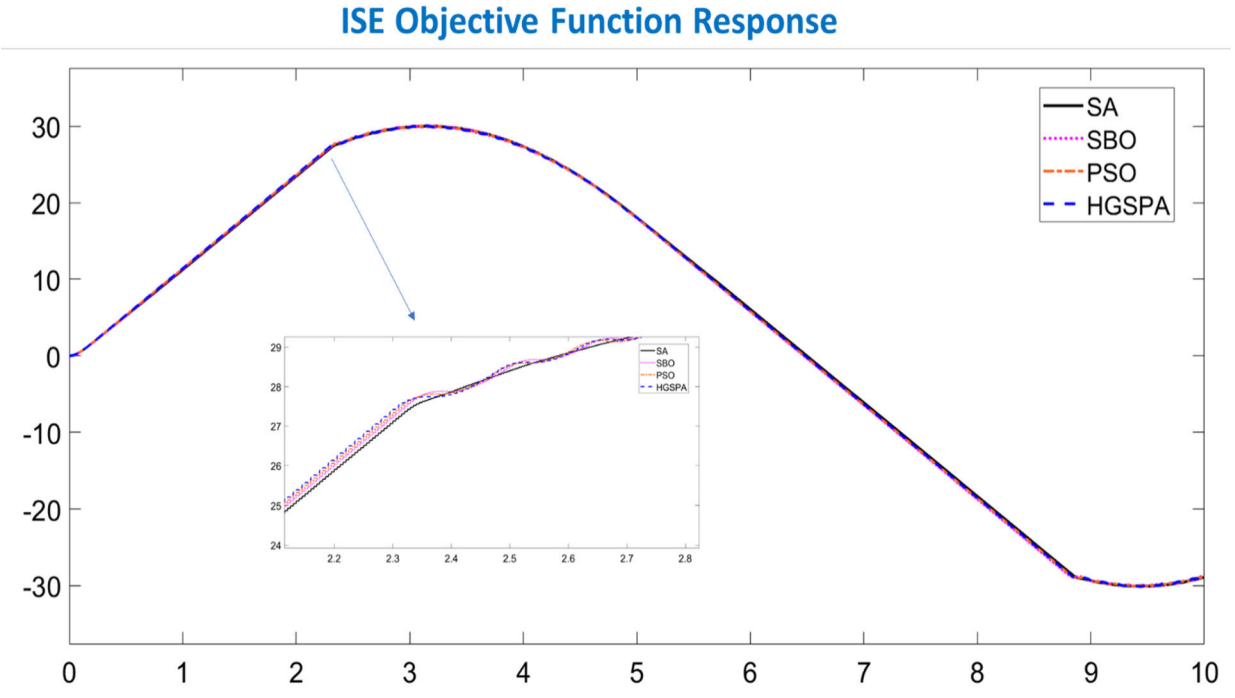

FIGURE 26. The experimental sine wave responses of different algorithms with the ISE objective function with 50 N load.

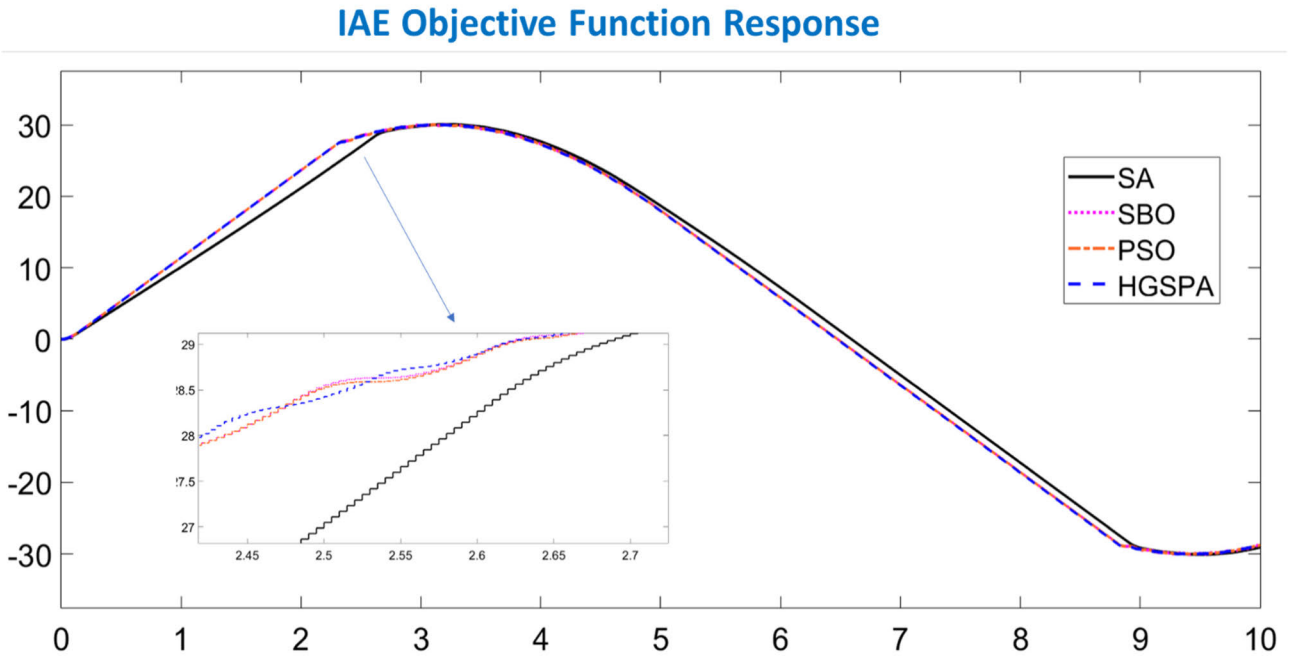

FIGURE 27. The experimental sine wave responses of different algorithms with the IAE objective function with 50 N load.

uration limits. For example, the good performance of SBO with ITAE in simulation results was different from the findings of the experiment due to high positive correcting torque. Moreover, with negligible overshoot and quick rise and settling times, the PSO algorithm with ITSE objective function provides an exceptional response.

To examine the system's robustness. A 50 N force was applied to the system. Using the ISE, IAE, ITSE, and ITAE objective functions with 50 cm as the system's reference input, the HGPSA, PSO, SA, and SBO transient responses with 50 N were obtained and are shown in Table 9. Figure 21 shows the transient responses of different algorithms with the ISE objective function, The transient responses of various

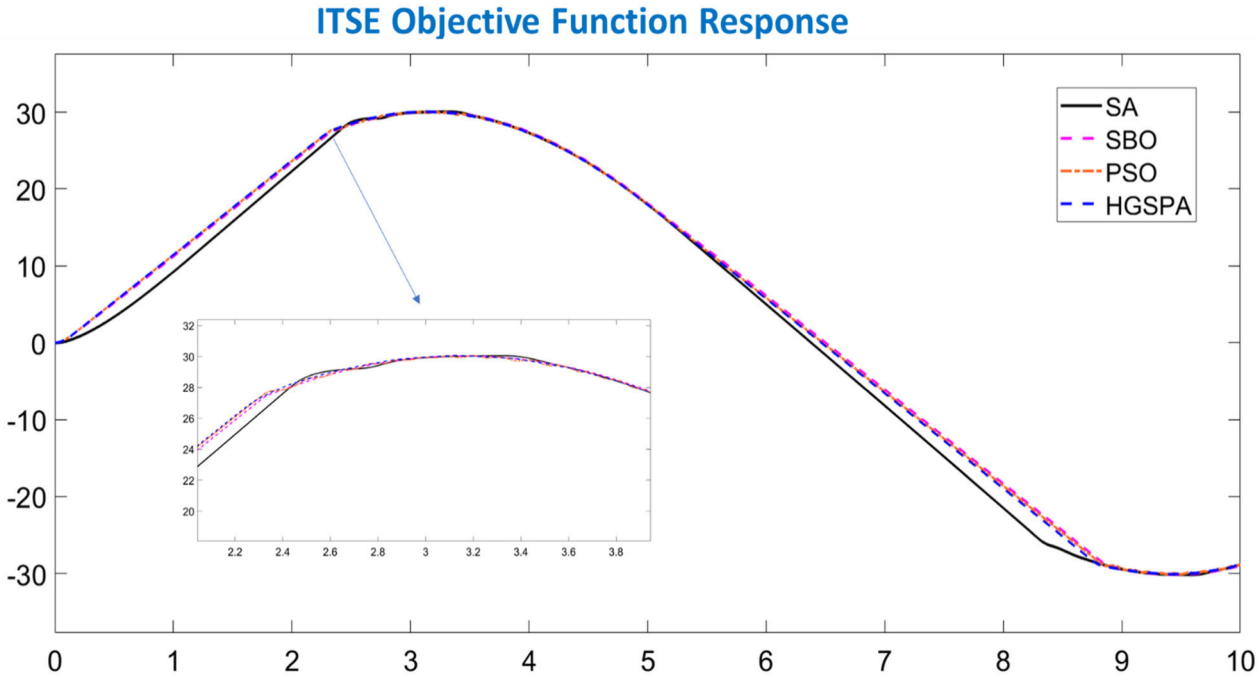

FIGURE 28. The experimental sine wave responses of different algorithms with the ITSE objective function with 50 N load.

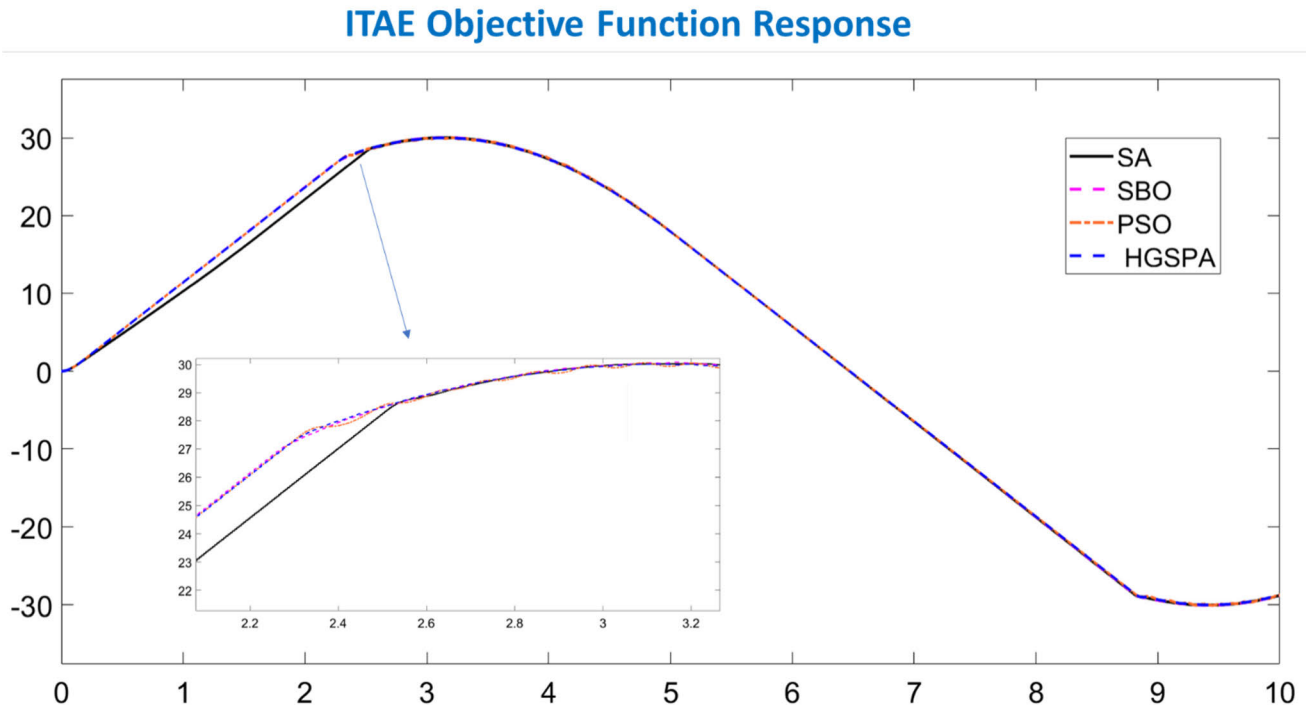

FIGURE 29. The experimental sine wave responses of different algorithms with the ITAE objective function with 50 N load.

algorithms with the IAE objective function are shown in Figure 22, those with the ITSE objective function are shown in Figure 23, and those with the ITAE objective function are shown in Figure 24.

The system exhibits outstanding stability and robustness during the 50 N load experiment test; however, weight addition causes a small increase in overshoot, rising time, and settling time. In experimental testing of SA with ITSE and ITAE objective functions as well as SBO with ITSE objective function, it is noticeable that the system responds very slowly. The primary cause of this is the low values of proportional gains in the outer and inner loops. Moreover,

experimental SBO testing with various objective functions results in a significant overshoot response.

In further tests to examine the system's robustness, a sine wave signal is input into the system with a 50 N load, as illustrated in Figure 25. Figure 26 shows the experimental sine wave responses of different algorithms with the ISE objective function, The experimental sine wave responses of various algorithms with the IAE objective function are shown in Figure 27, those with the ITSE objective function are shown in Figure 28, and those with the ITAE objective function are shown in Figure 29. The system's ITSE and ISE objective functions with SBO, PSO, and HGSPA algorithms produce outstanding results. A slow response with different objective functions is also generated by the SA algorithm.

V. CONCLUSION

In this paper, For the linear servo mechanism, a dynamic model was used in this study. The dynamic model was specifically built to minimize modeling errors and to ensure that any control techniques employed in the model experience the same challenges and conditions as the real model. Moreover, A PI-Cascaded control technique was used for the linear servo system which consists of two cascaded loops, each of which controls a different system component. The outer loop controls the system's linear position, whereas the inner loop controls the system's speed. Furthermore, four different meta-heuristic optimization algorithms (SBO, HGPSA, PSO, SA) with four different objective functions (ISE, IAE, ITSE, ITAE) were used to fine-tune the controller parameters. 50 cm was used as the system's reference input throughout the experimental testing of the system. The PSO algorithm with ITSE objective function has outstanding responsiveness with low overshoot (0 *cm*) and quick rising and settling durations (3.2231 *s and* 4.280 *s*).

On the other hand, experimental SBO testing using different objective functions causes an excessive overshoot response. To evaluate the robustness of the system. The system was subjected to a 50 N force. During the 50 N load experiment test, the system shows exceptional stability and robustness. The responses of the system in the simulation and experiment are comparable. Signal noise, encoder resolution restrictions, microcontroller specifications, disturbances, and PI saturation limits all contribute to a few variations, though. Moreover, a sine wave signal is input into the system with a 50 N load to test the stability and robustness of the system.

Future research initiatives are encouraged by the positive results that were found for this prototype. The system can use additional optimization approaches, such as the differential evolution algorithm. Additionally, several adaptive and machine learning-based controllers are proposed for use in future research to improve control responses under various loads. Additionally, this prototype may integrate more advanced functionalities like an inverted pendulum application.

REFERENCES

[1] I. M. Mehedi, M. H. M. Shah, and R. Jannat, "Linear positional and speed control of servo carts using inverse dynamic control," *Math. Problems Eng.*, vol. 2021, pp. 1–8, Aug. 2021, doi: 10.1155/2021/7411673.

[2] M. A. Shamseldin and M. A. Abdelghany, "A new self-tuning nonlinear PID motion control for one-axis servomechanism with uncertainty consideration," *J. Robot. Control (JRC)*, vol. 4, no. 2, pp. 118–127, Mar. 2023, doi: 10.18196/jrc.v4i2.17433.

[3] M. Abdullah-Al-Noman, A. N. Eva, T. B. Yeahyea, and R. Khan, "Computer vision-based robotic arm for object color, shape, and size detection," *J. Robot. Control*, vol. 3, no. 2, pp. 180–186, Feb. 2022, doi: 10.18196/jrc.v3i2.13906.

[4] H. Gao, A. Kareem, M. Jawarneh, I. Ofori, R. Raffik, and K. H. Kishore, "Metaheuristics based modeling and simulation analysis of new integrated mechanized operation solution and position servo system," *Math. Problems Eng.*, vol. 2022, pp. 1–7, Jun. 2022, doi: 10.1155/2022/1466775.

[5] G. B. Worku, "Autotransformer fed traction power supply system: Analysis, modeling and simulation," *Global Energy Interconnection*, vol. 1, no. 2, pp. 1–12, 2018.

[6] M. R. Islam and S. C. Banik, "Synchronizing of stabilizing platform mounted on a two-wheeled robot," *J. Robot. Control*, vol. 2, no. 6, pp. 1–12, 2021, doi: 10.18196/jrc.26136.

[7] H. Maghfiroh, M. Ahmad, A. Ramelan, and F. Adriyanto, "Fuzzy-PID in BLDC motor speed control using MATLAB/Simulink," *J. Robot. Control*, vol. 3, no. 1, pp. 8–13, Jun. 2021, doi: 10.18196/jrc.v3i1.10964.

[8] I. Suwarno, Y. Finayani, R. Rahim, J. Alhamid, and A. R. Al-Obaidi, "Controllability and observability analysis of DC motor system and a design of FLC-based speed control algorithm," *J. Robot. Control*, vol. 3, no. 2, pp. 227–235, Feb. 2022, doi: 10.18196/jrc.v3i2.10741.

[9] A. Jayachitra and R. Vinodha, "Genetic algorithm based PID controller tuning approach for continuous stirred tank reactor," *Adv. Artif. Intell.*, vol. 2014, pp. 1–8, Dec. 2014, doi: 10.1155/2014/791230.

[10] Y. Xie, J. Jin, X. Tang, B. Ye, and J. Tao, "Robust cascade path-tracking control of networked industrial robot using constrained iterative feedback tuning," *IEEE Access*, vol. 7, pp. 8470–8482, 2019, doi: 10.1109/ACCESS.2018.2889702.

[11] Y. Liu, M. A. Shah, A. Pljonkin, M. A. Ikbal, and M. Shabaz, "Design and research on the intelligent system of urban rail transit project based on BIM+GIS," *Scalable Comput., Pract. Exper.*, vol. 22, no. 2, pp. 1–13, Oct. 2021, doi: 10.12694/scpe.v22i2.1875.

[12] G. Dhiman, D. Oliva, A. Kaur, K. K. Singh, S. Vimal, A. Sharma, and K. Cengiz, "BEPO: A novel binary emperor penguin optimizer for automatic feature selection," *Knowl.-Based Syst.*, vol. 211, Jan. 2021, Art. no. 106560, doi: 10.1016/j.knosys.2020.106560.

[13] T. R. Biyanto, M. S. Alfarisi, N. Afdanny, H. Setiawan, and A. Hasan, "Simultaneous optimization of tuning PID cascade control system using Duelist algorithms," in *Proc. Int. Seminar Intell. Technol. Appl. (ISITIA)*, Lombok, Indonesia, 2016, pp. 601–606, doi: 10.1109/ISITIA.2016.7828728.

[14] S. Song, W. Cai, and Y.-G. Wang, "Auto-tuning of cascade control systems," *ISA Trans.*, vol. 42, no. 1, pp. 63–72, 2003, doi: 10.1016/S0019-0578(07)60114-1.

[15] M. Khosravi, V. Behrunani, R. S. Smith, A. Rupenyan, and J. Lygeros, "Cascade control: Data-driven tuning approach based on Bayesian optimization," *IFAC-PapersOnLine*, vol. 53, no. 2, pp. 382–387, 2020, doi: 10.1016/j.ifacol.2020.12.193.

[16] A. Nurettin, V. Ateş, and M. Lüy, "Tuning of PID controller for speed control of DC motor using genetic algorithm," *Int. J. Eng. Inf. Syst.*, vol. 6, no. 6, pp. 26–32, 2022.

[17] P. M. Meshram and R. G. Kanojiya, "Tuning of PID controller using Ziegler–Nichols method for speed control of DC motor," in *Proc. IEEE-Int. Conf. Adv. Eng., Sci. Manage.*, Mar. 2012, pp. 117–122.

[18] I. D. Fajuke and A. Raji, "Optimal tuning of PID controller for speed control of DC motor using equilibrium optimizer," *Indonesian J. Electr. Eng. Comput. Sci.*, vol. 30, no. 1, p. 89, Apr. 2023, doi: 10.11591/ijeecs.v30.i1.pp89-101.

[19] E. H. Dursun and A. Durdu, "Speed control of a DC motor with variable load using sliding mode control," *Int. J. Comput. Electr. Eng.*, vol. 8, no. 3, pp. 219–226, 2016, doi: 10.17706/IJCEE.2016.8.3.219-226.

[20] M. L. Hamida, H. Denoun, A. Fekik, and S. Vaidyanathan, "Control of separately excited DC motor with series multi-cells chopper using PI–Petri nets controller," *Nonlinear Eng.*, vol. 8, no. 1, pp. 32–38, Jan. 2019, doi: 10.1515/nleng-2017-0174.

[21] M. C. Rais, F. Z. Dekhandji, A. Recioui, M. S. Rechid, and L. Djedi, "Comparative study of optimization techniques based PID tuning for automatic voltage regulator system," *Eng. Proc.*, vol. 14, no. 1, p. 21, Feb. 2022, doi: 10.3390/engproc2022014021.

[22] A. Sharma, M. Fikar, and M. Bakosová, "Comparative study of time optimal controller with PID controller for a continuous stirred tank reactor," *Acta Chim. Slovaca*, vol. 8, no. 1, pp. 27–33, Apr. 2015, doi: 10.1515/acs-2015-0006.

[23] M. M. Gani, M. S. Islam, and M. A. Ullah, "Optimal PID tuning for controlling the temperature of electric furnace by genetic algorithm," *Social Netw. Appl. Sci.*, vol. 1, no. 8, p. 880, Aug. 2019, doi: 10.1007/s42452-019-0929-y.

[24] E. S. Rahayu, A. Ma'arif, and A. Çakan, "Particle swarm optimization (PSO) tuning of PID control on DC motor," *Int. J. Robot. Control Syst.*, vol. 2, no. 2, pp. 435–447, Jul. 2022, doi: 10.31763/ijrcs.v2i2.476.

[25] S. Kadry and V. Rajinikanth, "Design of PID controller for magnetic levitation system using Harris hawks optimization," *Jurnal Ilmiah Teknik Elektro Komputer Informatika*, vol. 6, no. 2, p. 70, Jan. 2021, doi: 10.26555/jiteki.v6i2.19167.

[26] S. Alghamdi, H. F. Sindi, M. Rawa, A. A. Alhussainy, M. Calasan, M. Micev, Z. M. Ali, and S. H. E. Abdel Aleem, "Optimal PID controllers for AVR systems using hybrid simulated annealing and gorilla troops optimization," *Fractal Fractional*, vol. 6, no. 11, p. 682, Nov. 2022, doi: 10.3390/fractalfract6110682.

[27] Y. Shimizu, "Efficiency optimization design that considers control of interior permanent magnet synchronous motors based on machine learning for automotive application," *IEEE Access*, vol. 11, pp. 41–49, 2023, doi: 10.1109/ACCESS.2022.3232857.

[28] M. Abdelbar, I. Mohamed, A. Abdellatif, and M. M. Hegaze, "Hybrid genetic algorithm-based optimal computed torque control of an upper-limb exoskeleton (SAMA)," Presented at the 32nd Int. Conf. Comput. Theory Appl., Dec. 2022.

[29] E. Köse, "Optimal control of AVR system with tree seed algorithm-based PID controller," *IEEE Access*, vol. 8, pp. 89457–89467, 2020, doi: 10.1109/ACCESS.2020.2993628.

[30] S. Habib, G. Abbas, T. A. Jumani, A. A. Bhutto, S. Mirsaeidi, and E. M. Ahmed, "Improved whale optimization algorithm for transient response, robustness, and stability enhancement of an automatic voltage regulator system," *Energies*, vol. 15, no. 14, p. 5037, Jul. 2022, doi: 10.3390/en15145037.

[31] S. K. Suman and V. K. Giri, "Speed control of DC motor using optimization techniques based PID controller," in *Proc. IEEE Int. Conf. Eng. Technol. (ICETECH)*, Coimbatore, India, Mar. 2016, pp. 581–587, doi: 10.1109/ICETECH.2016.7569318.

[32] G. A. Sultan and M. K. Jarjes, "Optimal PID controller design using artificial bee colony algorithm for robot arm," *Indonesian J. Electr. Eng. Comput. Sci.*, vol. 21, no. 1, p. 84, Jan. 2021, doi: 10.11591/ijeecs.v21.i1.pp84-91.

[33] M. J. Fotuhi, "Design and development of a ball-screw and electrical motor driven industrial electromechanical cylinder," *Sigma J. Eng. Natural Sci.*, vol. 2022, pp. 1–10, Mar. 2022, doi: 10.14744/sigma.2022.00098.

[34] M. Dooley and X. Shen, "A novel self-actuated linear drive for long-range-of-motion electromechanical systems," *Actuators*, vol. 11, no. 9, p. 250, Sep. 2022, doi: 10.3390/act11090250.

[35] X. Liu, Z. Wang, and X. Wang, "Full prediction cascade control of permanent magnet toroidal motor with time-varying parameters," *Trans. Inst. Meas. Control*, vol. 2023, Jan. 2023, Art. no. 014233122211395, doi: 10.1177/01423312221139585.

[36] M. Abdelbar, I. Mohamed, A. Abdellatif, and M. M. Hegaze, "Towards the mechatronic development of a new upper-limb exoskeleton (SAMA)," *Designs*, vol. 6, no. 5, p. 80, Sep. 2022, doi: 10.3390/designs6050080.

[37] Z. Yudong and W. Lenan, "Bacterial chemotaxis optimization for protein folding model," in *Proc. 5th Int. Conf. Natural Comput.*, 2009, pp. 159–162, doi: 10.1109/ICNC.2009.190.

[38] T. T. Anh, N. In-Seop, and K. Soo-Hyung, "A hybrid method for table detection from document image," in *Proc. 3rd IAPR Asian Conf. Pattern Recognit. (ACPR)*, Nov. 2015, pp. 131–135, doi: 10.1109/ACPR.2015.7486480.

[39] C. L. Lok, B. Vengadaesvaran, and S. Ramesh, "Implementation of hybrid pattern search–genetic algorithm into optimizing axial-flux permanent magnet coreless generator (AFPMG)," *Electr. Eng.*, vol. 99, no. 2, pp. 751–761, Jun. 2017, doi: 10.1007/s00202-016-0443-9.

[40] A. G. Gad, "Particle swarm optimization algorithm and its applications: A systematic review," *Arch. Comput. Methods Eng.*, vol. 29, no. 5, pp. 2531–2561, Aug. 2022, doi: 10.1007/s11831-021-09694-4.

[41] A. B. Ceylan, L. Aydın, M. Nil, H. Mamur, İ. Polatoğlu, and H. Sözen, "A new hybrid approach in selection of optimum establishment location of the biogas energy production plant," *Biomass Convers. Biorefinery*, vol. 13, no. 7, pp. 5771–5786, May 2023, doi: 10.1007/s13399-021-01532-8.

[42] Z.-H. Han and K.-S. Zhang, "Surrogate-based optimization," in *Real-World Applications of Genetic Algorithms*, O. Roeva, Ed. Rijeka, Croatia: InTech, 2012, doi: 10.5772/36125.

[43] H. M. Gutmann, "A radial basis function method for global optimization," *J. Global Optim.*, vol. 19, no. 3, pp. 201–227, 2001.

[44] H. Xu, T. Zhang, Y. Luo, X. Huang, and W. Xue, "Parameter calibration in global soil carbon models using surrogate-based optimization," *Geosci. Model Develop.*, vol. 11, no. 7, pp. 3027–3044, Jul. 2018, doi: 10.5194/gmd-11-3027-2018.

[45] S. Ekinci and B. Hekimoglu, "Improved kidney-inspired algorithm approach for tuning of PID controller in AVR system," *IEEE Access*, vol. 7, pp. 39935–39947, 2019, doi: 10.1109/ACCESS.2019.2906980.

[46] T. Kumbasar and H. Hagras, "Big bang–big crunch optimization based interval type-2 fuzzy PID cascade controller design strategy," *Inf. Sci.*, vol. 282, pp. 277–295, Oct. 2014, doi: 10.1016/j.ins.2014.06.005.

[47] N. S. Ozbek and İ. Eker, "A novel modified delay-based control algorithm with an experimental application," *Inf. Technol. Control*, vol. 48, no. 1, pp. 90–103, Mar. 2019, doi: 10.5755/j01.itc.48.1.19066.

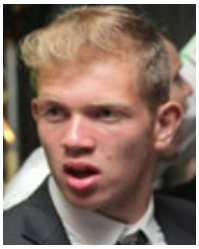

M. ABDELBAR received the B.Sc. degree in mechatronics engineering and the M.Sc. degree in mechanical engineering from the Arab Academy for Science, Technology and Maritime Transport (AASTMT), Egypt, in 2019 and March 2023, respectively. He graduated with a 3.98 GPA, which was the highest GPA among graduating students. He is currently an Assistant Lecturer at AASTMT Smart Village Campus. His research interests include non-linear system control, optimization applications, wearable robots, and collaborative robot control.

HUDA RAMADAN was born in Egypt. She received the bachelor's degree in mechanical engineering from the Arab Academy for Science, Technology, and Maritime Transport (AASTMT), in 2023. She specialized in mechatronics engineering and achieved a GPA of 3.8. Throughout her academic journey, she gained practical experience through internships at prestigious organizations. She is currently actively involved in ongoing research aimed at optimizing the performance of a PID controller for a linear servo mechanism. With a background in embedded software and control systems, she demonstrates a keen interest in these fields.

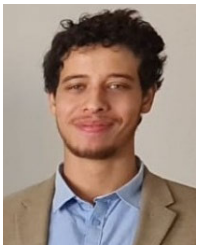

ABDELRAHMAN KHALIL was born in Cairo, Egypt. He is currently pursuing the bachelor's degree in mechatronics engineering with the Arab Academy for Science, Technology, and Maritime Transport (AASTMT). He has worked on various projects that involved PID control and especially on linear servo mechanisms. His current research interest includes optimization control of cascaded PID of a linear servo mechanism.

HAMAD FARAG is a results-driven Mechatronics Engineer with some experience in designing, developing, and testing robust software solutions. He graduated with a 3.7 GPA from the Arab Academy for Science, Technology, and Maritime Transport, class of 2023. He was interested in robotics and control projects and worked on "Design, Modelling, and Fabrication of Quadruped" for my graduation project.

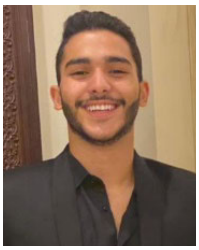

MAZEN BAHGAT was born in Egypt. He received the bachelor's degree in mechanical engineering from the Arab Academy for Science, Technology, and Maritime Transport (AASTMT), in 2023. He specialized in mechatronics engineering. He is a dedicated Mechatronics Engineer professional with a history of meeting company goals utilizing consistent and organized practices. He is skilled in working under pressure and adapting to new situations and challenges to best enhance the organizational brand. He has previously worked on several embedded systems and automation projects which included low-level and high-level control.

OMAR RABIE was born in Egypt. He received the bachelor's degree in mechanical engineering from the Arab Academy for Science, Technology, and Maritime Transport (AASTMT), in 2023. He specializes in control systems, mathematical optimization, and modeling. The goal of his work and research is to close the gap between mathematical models and real-life hardware systems, although insignificant in magnitude, in effect, it can make a huge difference.

YASSER EL-SHAER received the B.Sc. degree in mechanical power engineering and the M.Sc. degree in mechanical engineering (fracture mechanics) from the Military Technical College, Cairo, Egypt, in 1992 and 1998, respectively, and the Ph.D. degree in mechanical engineering from the Manchester Materials Science Centre (UMIST), Manchester, U.K., in 2003. In 2013, he joined the Thermodynamics of Materials Research Group, Concordia University. Since 2019, he has been an Associate Professor and the Head of the Mechanical Engineering Department (Mechatronics), AAST&MT, Smart Village Campus, Giza, Egypt. His research interests include mechanical design, engineering optimization, engineering measurements, and nonlinear stress analysis and simulation.